9.06 Plate Tectonics through Time

N. H. Sleep, Stanford University, Stanford, CA, USA

© 2007 Elsevier B.V. All rights reserved.

9.06.1 Introduction

The scientific issues that arose during the advent of the theory of plate tectonics place the modern issue of tectonics on the early Earth in context. The existence of seafloor spreading in the Atlantic and ridge–ridge transform faults were established when the author attended his first international scientific conference at Woods Hole in the summer of 1967. Later, the approximation of rigid plates on a spherical shell provided the global geometry, taking advantage of transform faults. Subduction provided an explanation of deep-focus earthquakes and the sink for the oceanic lithosphere produced by seafloor spreading. It was evident at the Woods Hole meeting that no one there had any idea how seafloor spreading works. This lacuna did not greatly concern the mainly observational scientists in attendance.

The initial hypothesis explained continental drift, relegating continents to plate passengers. Atwater (1970) brought the concept ashore in California demonstrating its great explicative power to continental tectonics. Overall, the plate tectonic revolution shifted attention away from cratons. Yet the interior of continents had geological records of real events.

In December 1975, the author attended the Penrose Conference on continental interiors, the final stationary bastion under siege. Fixists hijacked the conference, jettisoned the published program, and mounted a determined counterattack. Speaker after speaker droned on that his locality was very complicated, that plate tectonics was of no use in interpreting the geology, that it certainly could not be established just looking at his quadrangle, and thus that the theory is dead wrong.

With regard to tectonics in the Earth's deep past, we are much like land-based geologists in 1975. The biases of geological preservation place us in the same bind that provincial data selection placed the Penrose holdouts during that freezing December in San Diego. We have little intact seafloor older than the ~180 Ma crust along the passive margins of the central Atlantic (Moores, 2002). We cannot observe the lynchpins of modern plate tectonics, magnetic stripes, and ridge–ridge transform faults. We certainly cannot observe earthquake mechanisms, the geoid, and tomography. Essentially, we are stuck

with data from continents, the very regions that befuddled earlier geologists.

Yet we can do better with the deep past than Earth science did with the Tertiary in 1960. We can view geology at appropriate scales with the caveat that later tectonics dispersed the Archean record into ~35 blocks (Bleeker, 2003). We have a reasonable understanding of the kinematics of modern Earth, especially the record-producing process of continental breakup eventually followed by continental collision. Geodynamicists picked much of the low-hanging fruit from the orchard opened by plate tectonics over the last 40 years. We know how the modern Earth works well enough that we have hope of exporting concepts in time and to other planets.

Export inflicts some discussion of semantics. Plate tectonics, as originally conceived, was an approximate kinematic theory. It unified continental drift, seafloor spreading, subduction, and transform faulting. Orogeny from continental collision provided an apt explanation of mountain belts. These processes are linked but somewhat disjoint. For example, seafloor spreading does not kinematically require that the plates are rigid, that subduction is one-sided, or even that transform faults exist. Mantle plumes and thick cratonal lithosphere are significant features on the modern Earth that are further afield from plate processes.

With regard to the cardinal kinematic postulate, rigid plates tessellate 85% of the Earth's surface (e.g., Zatman *et al.*, 2005). Diffuse plate boundaries grout the remainder. Diffuse deformation zones divide major oceanic plates into subplates. Typically, the pole of rotation for the two subplates lies near their boundary so that both extension and compression occur. This process may nucleate subduction, but otherwise is lost in the fog of time. Diffuse continental zones, like the Basin and Range, the Lena River region of Siberia, and Tibet occur within hot weak continental crust. Both extension and compression have high preservation potential including sediments, focusing attention on vertical tectonics.

Continental collisions, like India with Tibet, produce strike-slip faults that extend far inland from the point of indention (Molnar and Tapponnier, 1975). The faults disrupt the orogen as well as otherwise stable regions. The record has a high preservation potential that is readily associated with the plate processes.

In all cases, vertical tectonics is more easily recognized than strike-slip tectonics. This is especially true with continent-margin-parallel faults, like the San Andreas Fault and the fault system through the Sumatra volcanic arc. Lateral offset is not obvious because the fault runs along the gross geological strike. Piercing points may be quite distant. Recently uplifted mountain ranges (e.g., in western California) are more evident than the strike-slip component of the tectonics. Historically, this view seemed natural; the US Geological Survey topographic map of Palo Alto perpetuates the archaic term, the San Andreas Rift.

The question of the antiquity of plate processes arose soon after geologists accepted the modern process (Hurley and Rand, 1969). A significant literature exists. The reader is referred to the works of Sleep (1979, 1992) and Sleep and Windley (1982) for discussions of early work. Stevenson (2003) and Korenaga (2006) discuss ancient global dynamics. Bleeker (2003), Sleep (2005), Condie and Benn (2006), and Polat and Kerrich (2006) review the rock record on continents. Moores (2002) reviews possible exposures of ancient oceanic crust. On the other hand, Stern (2005) argues that modern plate processes began in Neoproterozoic time.

The author winnows the subset of geodynamic theory and geological observation that bears on the problem at hand, begins with convection to put the physics in context, and then moves forward in time from the Earth's formation for first evidence of various aspects of plate tectonics. He then considers changes in the more recent past, finally considering the fate of the Earth in the geological future.

This chapter relates to many topics in this *Treatise on Geophysics*. Volumes 6 and 7 relate to the current state of the Earth. In this volume, Chapters 9.04, 9.09, 9.07, and 9.01 cover topics that are intimately coupled with this chapter.

9.06.2 Physical Preliminaries

Plate tectonics is a form of convection where hot material rises at ridges and cold dense slabs sink. Much of geodynamics involves this heat and mass transfer process. This chapter reviews the physics in this section so that it can be referred back when the the Earth's history is discussed.

Since the nature of convection within the Earth changed over time, we loosely divide early Earth history into the period immediately after the Earth's formation, part of the Hadean where a 'magma' ocean filled with mostly crystalline 'mush' covered the

planet, and the Archean 2.5–3.8 Ga , where it becomes meaningful to compare theory and observation. After the Archean, we can apply analogies to modern plate processes with more confidence to a reasonable record.

The Earth's mantle is complicated. Plate boundaries fail by faulting. The interior creeps as a very viscous fluid. Partial melting produces buoyant oceanic crust. These processes are complex enough that examination of the rock record is essential. It is useful to see the bases of common physical arguments about the tectonics of the Earth. This chapter begins with a discussion on the heat balance in the mantle.

9.06.2.1 Global Heat Balance

One can construct a thermal history of the Earth's interior by equating surface heat flow with contributions from transient cooling and radioactive heat generation. Formally, the heat balance for the mantle is

$$4\pi r_E^2 q = \frac{4\pi\left(r_E^3 - r_C^3\right)}{3}\rho H - \frac{4\pi r_E^3}{3}\rho C\frac{\partial T}{\partial t} + 4\pi r_c^2 q_C \qquad [1]$$

where q is the heat flow from the mantle, r_E is the Earth's radius, q_C is the heat flow at the core's radius r_C, ρ is density, C is specific heat (essentially at constant pressure), H is radioactive heat generation per mass, T is the interior mantle temperature, and t is time. We make an approximation that the core cools at the same rate as the mantle in example calculations. About one-fifth of the Earth's heat capacity is in the core so its details can be ignored in some qualitative arguments but certainly not those related to plumes.

The specific heat of the mantle is about $1.25\,\mathrm{J\,K^{-1}\,kg^{-1}}$. This implies that a global heat flow of $1\,\mathrm{W\,m^{-2}}$ cools the mantle at $3.2\,\mathrm{K\,My^{-1}}$. Heat flows greater than this quickly cool the mantle and cannot have been sustained through even the Hadean. The present mantle heat flow of $0.070\,\mathrm{W\,m^{-2}}$ would cool the mantle at 225 K per billion year and the whole Earth at 180 K per billion year. A major task in geodynamics is to obtain the average surface heat flow as a function of the interior temperature, which leaves radioactivity as the unknown quantity in [1].

This chapter presents the results of simple thermal models of the Earth's history at this stage for use throughout this chapter. The intent is to put potentially geologically observable features and geodynamics in a common context. The models conserve energy using eqn [1]. The globally averaged heat flow is a multibranched function of the interior temperature. The computed thermal evolution of the Earth is a trajectory as shown in this graph (**Figure 1**). The models generate physically realizable thermal histories, not cartoons. See Appendix 1 for the parameters used to compute these semischematic graphs.

Radioactive decay and the cooling of the Earth's interior over time are now comparable items in the Earth's heat budget. In example calculations, the current heat flow supplied by radioactivity is half the total (i.e., $0.035\,\mathrm{W\,m^{-2}}$). (We use extra digits throughout this chapter to make calculations easier to follow.)

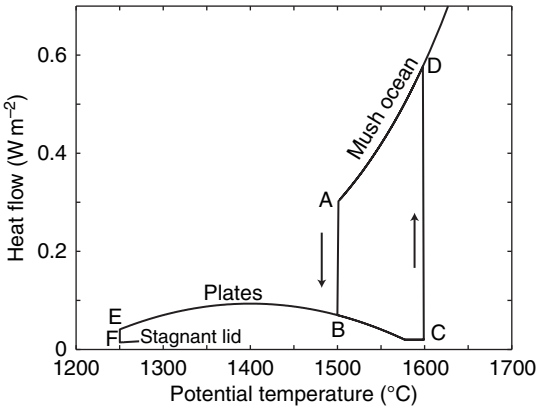

Figure 1 The heat flow from the Earth's mantle is a multibranched function of the potential temperature of the Earth's interior. Thermal histories are paths on this graph. One model has a monotonic thermal history where the heat flow lies along the transition in branch jumps. The other model jumps between branches and has a nonmonotonic thermal history. Both models start at 2000°C at 4.5 Ga. The mantle cools along the mush-ocean path until it reaches point A. The nonmonotonic model jumps to plate tectonics at point B. If the heat flow is greater than the radioactive heat generation, the mantle cools along the plate branch moving toward point E. If the heat flow is lower than the radioactive heat generation, the mantle heats up to point C, where convection jumps to the mush-ocean branch at point D. It then cools to point A. The nonmonotonic model jumps to stagnant-lid convection from point E to F. The mantle then heats up. The monotonic model stays at the jumps with the heat flow equal to radioactive heat generation until radioactive heat generation decreases to heat flow of the cooler mode. Note Thom (1983) popularized this presentation method in his catastrophe theory. The author eschews the word 'catastrophe' in the text as it is pre-empted with a foul stench in the Earth sciences. One could add another axis perpendicular to the plane of the diagram. Continental area would be a good choice (Lenardic *et al.*, 2005). One would then need the net growth (shrinkage) rate of continents as a function of interior temperature, convection mode, and continental area to compute forward models.

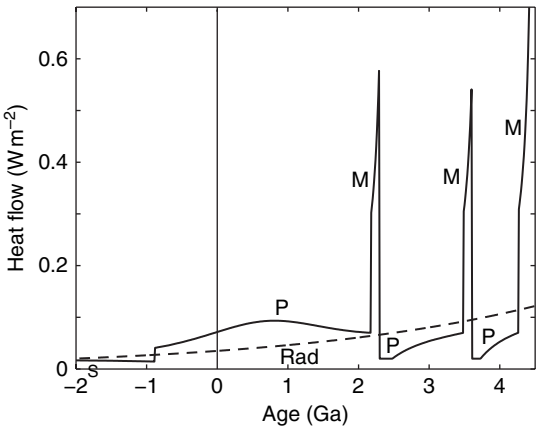

Figure 2 Computed heat flow as a function of age for the nonmonotonic model (dark line) and the radioactive heat generation as heat flow (thin dashed line). The modes of convection are (M) mush ocean, (P) plates, and (S) stagnant lid. The model resolves the expected duration of episodes, but no attempt was made to fine-tune the timing of transitions.

This heat flow is somewhat higher than the bulk silicate Earth model estimate of 0.024 W m^{-2}. The heat flow from radioactivity at 4 Ga was a factor of a few more than present (i.e., ~0.13 W m^{-2} in the examples presented here) (**Figure 2**). (Negative ages are in the future.) About one-third of the radioactivity is currently at shallow depths within continental crust where it does not drive mantle convection. Continent-like chemical reservoirs existed by ~4.5 Ga (Harrison *et al.*, 2005), but the ancient fraction of radioactivity sequestered within continents in the deep past is unknown. We use the current partition in examples, as the exact amount does not affect the gist of the arguments (**Figure 2**). Antineutrino detectors soon will provide hard data on the absolute abundance of U and Th in the Earth's interior (Araki *et al.*, 2005; Fiorentini *et al.*, 2005; Sleep, 2006). For simplicity, we also ignore the direct effect of continental area on the vigor of convection (Lenardic *et al.*, 2005).

9.06.2.2 Heat Transfer by Seafloor Spreading

The global heat balance provides necessary attributes for whatever type of global tectonics existed in the Later Hadean and the Archean. Radioactive heat production was small enough that plate tectonics is a viable candidate mechanism. As at present, one needs to consider the main mechanism of heat transfer, the formation, and cooling of oceanic lithosphere.

One obtains simple well-known formulas by considering the oceanic lithosphere to be a half-space (e.g., Turcotte and Schubert, 1982). We present their first-order forms in one place so that we may refer back to them later. The roof of a liquid or mush-filled magma ocean might well cool as a plate above an isothermal half-space.

We use global spreading rate U, the global production rate of new seafloor at ridges, conveniently given in km^2 yr^{-1}. The time for seafloor spreading to renew the Earth's surface is then $t_E \cong 4\pi r_E^2/U$. This time represents the age of old seafloor at the time of subduction; we use the subduction age and the renewal time interchangeably in dimensional arguments. The present global spreading rate is ~3 km^2 yr^{-1}, which would resurface the ocean basins in ~100 My and the Earth in 170 My White *et al.* (1992) give a more precise estimate of 3.3 km^2 yr^{-1}.

The global average heat flow depends on the square root of the renewal time

$$q = \frac{2k\Delta T}{\sqrt{\pi\kappa t_E}} \qquad [2]$$

where ΔT is the temperature contrast between the surface and the hot mantle beneath the lithosphere, k is thermal conductivity, ρ is density, and $\kappa \equiv k/\rho C$ is thermal diffusivity. The current average heat flow in the ocean basins is ~0.10 W m^{-2}, comparable to radioactive heat generation in the Archean. Radioactivity alone thus does not mandate a very vigorous form of Archean convection.

Other simple relationships bear on geodynamics. Plate thickness of the oldest lithosphere scales as

$$L = \sqrt{\kappa t_E} \qquad [3]$$

For quick calibration, 1 My lithosphere is ~10 km thick. The elevation of buoyant ridges relative to old oceanic crust produces 'ridge push,' a driving force for seafloor spreading. The membrane stress (the difference between horizontal stress and the vertical stress from lithostatic pressure) scales as

$$\tau = \rho g \alpha \Delta T (\kappa t_E)^{1/2} \qquad [4]$$

where g is the acceleration of gravity and α is the volume thermal expansion coefficient. Stress is concentrated within the cool brittle upper part of the lithosphere. The integral of this stress over the thickness of the lithosphere is the 'ridge push' force available to drive plate motion. It is

$$F = \tau L = \rho g \alpha \Delta T (\kappa t_E) \qquad [5]$$

The negative buoyancy of downgoing slabs is the other major driver of plate motions.

9.06.2.3 Parametrized Convection

Equation [1] can be integrated forward or back in time if one has the surface heat flow as a function of the interior temperature (**Figures 1** and **3**) and the concentrations of heat-producing elements (**Figure 2**). From [2], knowing the rate of convection as a function of interior temperature suffices. To do this, we assume that the vigor of convection depends only on the properties of the lithosphere and the uppermost asthenosphere, not those of the deep mantle; that is, the global convective heat flow depends on the temperature at the base of the lithosphere and the fraction of the Earth's surface covered by continental crust (Lenardic *et al.*, 2005). The convective heat flow does not depend on the instantaneous rate of radioactive heat generation.

Fluid dynamists call these assumptions 'boundary layer theory'. It applies in general if the thermal boundary layers comprise a small fraction of the total thickness of the convecting region. The Earth meets this criterion; the lithosphere is much thinner than the mantle.

We briefly review rheology to put the remaining discussion in context. In full tensor form, the strain rate in an isotropic material is

$$\varepsilon'_{ij} = \frac{\tau_{ij}\tau^{n-1}}{2\eta\tau_{\text{ref}}^{n-1}} \qquad [6]$$

where η is the viscosity, τ_{ij} is the deviatoric stress tensor (the stress that produces shear, mathematically the stress tensor with zero trace), the scalar stress τ is the second invariant of the stress tensor $\sqrt{\tau_{ij}\tau_{ij}}$ (appropriately normalized it is the resolved shear stress in two dimensions), n is the exponent of a power-law rheology, and τ_{ref} is a reference stress that may be chosen for convenience. The scalar form is useful for dimensional calculations:

$$\varepsilon' = \frac{\tau^n}{\eta\tau_{\text{ref}}^{n-1}} \qquad [7]$$

The familiar linear or Newtonian fluid is the case where $n = 1$. A plastic substance fails at a yield stress. This corresponds to the limit $n \to \infty$. We present applications of parametrized convection in the order that their relevancies arose in the Earth's history.

A linearly viscous fluid reasonably represents liquid magma and hence the liquid magma ocean on the early Earth. It may represent convecting mush and the present asthenosphere. The formalism for this rheology illustrates key aspects of the parametrized convection approach before we discuss nonlinear $n < 1$ rheology. The convective heat flow is then

$$q = Ak\Delta T\left[\frac{\rho C g\alpha\Delta T}{\kappa\eta}\right]^{1/3} \qquad [8]$$

The dimensionless multiplicative constant A is of the order of 1; it depends on the upper boundary condition. ΔT is the temperature contrast that actually drives convection and η is the viscosity of the conducting interior (Davaille and Jaupart, 1993a, 1993b, 1994; Solomatov, 1995; Solomatov and Moresi, 2000). These two quantities are the dominant terms in [8]. Temperature contrast is raised to the 4/3 power. Viscosity decreases orders of magnitude with increasing temperature.

The linear rheology assumed in [8] does not apply to plate tectonics because trench and transform boundaries fail in friction rather than viscous flow. One approach is to apply the parametrized formula for a nonlinear fluid:

$$q = A_n k\Delta T\left[\frac{\Delta T^n(\rho g\alpha)^n}{\kappa\tau_{\text{ref}}^{n-1}\eta}\right]^{1/(n+2)} \qquad [9]$$

where the full temperature contrast ΔT across the lithosphere drives convection. The dimensionless multiplicative constant A_n depends both on the exponent n and the boundary conditions. As one approaches the limit of a plastic rheology $n \to \infty$, the heat flow becomes independent of the viscosity η and proportional to square of the temperature

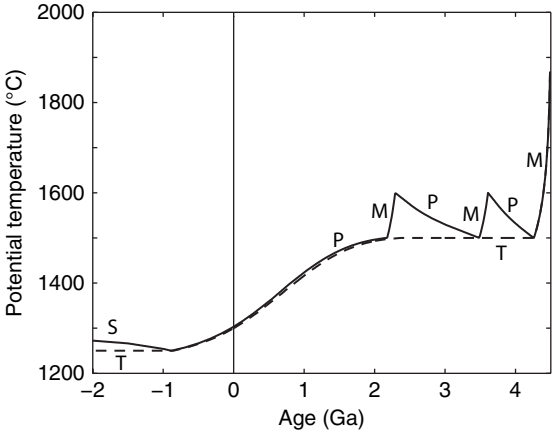

Figure 3 The computed thermal history for the nonmonotonic model (dark line) and the monotonic model (thin dashed line). The modes of convection are mush ocean (M), plates (P), stagnant lid (S), and transition (T) in the monotonic model. The temperature remains constant in the transitions in the monotonic model.

contrast. This inference assumes correctly that the yield stress does not depend greatly on temperature; the 'brittle' strength of plates is concentrated at cool shallow depths (e.g., Zoback and Townend, 2001). Plate-bounding faults, such as the San Andreas Fault, are much weaker than 'normal' rocks failing in friction at hydrostatic pore pressure.

We derive this temperature-squared relationship by letting τ in [4] represent the plastic yield stress τ_Y, where

$$\tau_Y = \rho g \alpha \Delta T (\kappa t_E)^{1/2} \qquad [10]$$

Solving [2] and [10] by eliminating the resurfacing time t_E yields the heat flow

$$q = \frac{2k\rho\alpha g \Delta T^2}{\tau_Y \sqrt{\pi}} \qquad [11]$$

As discussed in Section 9.06.3, the Earth's interior cooled only a few 100 K since a solid lithosphere formed. For example, the heat flow in [11] when the interior was 1800°C versus 1300°C at present was only a factor of $(1800/1300)^2 = 1.9$ greater than present.

Stagnant-lid convection occurs beneath the lithosphere because viscosity is strongly temperature dependent (**Figure 4**). As discussed in Section 9.06.5, it will become the mode of convection within the Earth in the geological future. It is now the mode of convection within Mars and Venus. The cooler upper part of the lithosphere is essentially rigid on those planets (*see* Chapter 10.13).

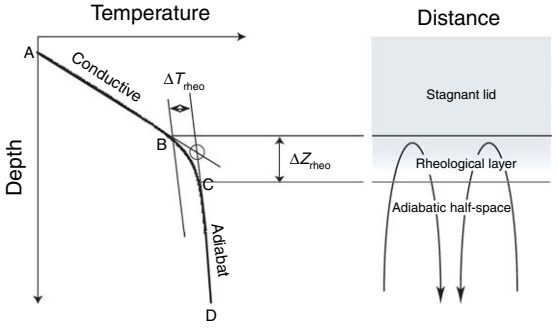

Figure 4 Schematic diagram of stagnant-lid convection at the base of the lithosphere. The geotherm (dark line, left side) has a linear conductive gradient (A to B) within the stagnant lid. It is adiabatic (C to D) below the stagnant lid. The rheological boundary layer is the top of convection (right). The geotherm changes form conductive at B to abiabat at C. The geothermal gradient in the region scales as ~1/2 the conductive gradient. The high viscosity near the top of the rheological layer limits the flow rate.

Only a thin rheological boundary layer actually partakes in convection (**Figure 4**). The temperature contrast across the layer determines whether underlying convection impinges on the base of the crust. In laboratory and numerical experiments, the viscosity contrast between the top of the rheological boundary layer and the underlying half-space is a factor ~10 for a linear fluid. Simple convenient expressions arise when we represent viscosity in a traditional form,

$$\eta = \eta_{ref} \exp\left[\frac{T_{ref} - T}{T_\eta}\right] \qquad [12]$$

where η_{ref} is the reference viscosity at temperature T_{ref} and T_η is the temperature scale for viscosity. The parametrized convection equation [9] in general becomes

$$q = A_n k T_\eta \left[\frac{T_\eta^n (\rho g \alpha)^n}{\kappa \tau_{ref}^{n-1} \eta}\right]^{1/(n+2)} \qquad [13]$$

where the viscosity is that of the underlying half-space and the reference stress may be defined for convenience. The temperature contrast of the rheological boundary layer is

$$\Delta T_{rheo} \approx 1.2(n+1) T_\eta \qquad [14]$$

Stagnant-lid convection today supplies modest amounts of heat flow to the base of the oceanic lithosphere. It supplies the bulk of the heat flow through stable continental lithosphere. The asthenosphere and the rheological boundary layer beneath these regions may well behave as a linearly viscous fluid. The temperature scale T_η is not precisely known; 43 K (which provides an order of magnitude over 100 K) is a venerable approximation. It could be as high as 100 K. The temperature contrast of the rheological boundary layer is less than a few hundred kelvin. Stagnant-lid convection does not impinge on the base of the crust within stable parts of the continent.

9.06.2.4 Changes in the Mode of Convection

The mode of convection in the Earth changed a few times. Changes included mush-filled magma ocean to plate tectonics. (The traditional term 'magma ocean' misleadingly implies a fully molten reservoir. The nonstandard term 'mush ocean' is preferable as it implies a region of mostly crystalline mush.) Convection may have conceivably gone from plate tectonics back to mush ocean. Transition from plate

tectonics to stagnant-lid convection is inevitable in the geological future. The initiation of subduction and the delamination of the base of the lithosphere are local mode changes. ('Delamination' is massive foundering of cold dense mantle lithosphere into the underlying mantle.)

This chapter illustrates a general formalism for representing mode changes involving stagnant-lid convection. The physical processes involve the fact that the strain rate within the lithosphere depends nonlinearly on stress. We do not have a quantitative form for transitions involving a mush ocean (See Appendix 2).

To derive [14], Solomatov and Moresi (2000) presumed that stagnant-lid convection self-organizes the rheological temperature contrast ΔT_{rheo} so that flow transports the maximum convective heat flow. We illustrate this property qualitatively before doing mathematics. The convective heat flow depends on the product of the flow rate and the rheological temperature contrast. If the rheological temperature contrast is very small, little heat gets transferred because no temperature variations are available to transfer heat and the buoyancy forces driving convection are quite small. Conversely, there are ample buoyancy forces and temperature variations if the rheological temperature contrast is very large, but the high viscosity of the cool material in the stagnant lid precludes flow. The maximum convective heat flow exists in between where there are both temperature variations and a viscosity only modestly higher than that of the underlying half-space. Laboratory and numerical calculations show that the following formalism provides reasonable predictions of the rheological temperature contrast.

We continue with mathematics, extending the form of the derivation by Sleep (2002) to a more complicated rheology. To keep equations as compact as possible, we assume that linear and nonlinear creep mechanisms act in parallel and use the scalar form [7] to obtain dimensional results. The scalar strain rate is then

$$\varepsilon' = \frac{\tau}{\eta} + a\frac{\tau^n}{\eta\tau_{\text{ref}}^{n-1}} \qquad [15]$$

where a is a dimensionless constant. In general, the temperature dependence of the two creep mechanisms may differ and the stress–strain rate relationship may be more complex.

We make the rheological temperature contrast ΔT_{rheo} a free parameter with the intent of outlining the derivation of [14] by finding its maxima in the convective heat flow (**Figure 5**). The thickness of the rheologically active layer is then (**Figure 4**)

$$\Delta Z_{\text{rheo}} = \Delta T_{\text{rheo}}\left(\frac{\partial T}{\partial Z}\right)^{-1} \qquad [16]$$

where $\partial T/\partial Z$ is the thermal gradient. The stress from lateral variations of temperature scales with the product of the density contrast within the rheological boundary layer and its thickness. The stress within the rheological layer is dimensionally

$$\tau \approx \rho g \alpha\, \Delta T_{\text{rheo}}^2\left[\frac{\partial T}{\partial Z}\right]^{-1} \qquad [17]$$

Note that [4] arises from the analogous product of density contrast with lithosphere thickness.

The velocity in the thermal boundary layer is the integral of the strain rate across the rheologically

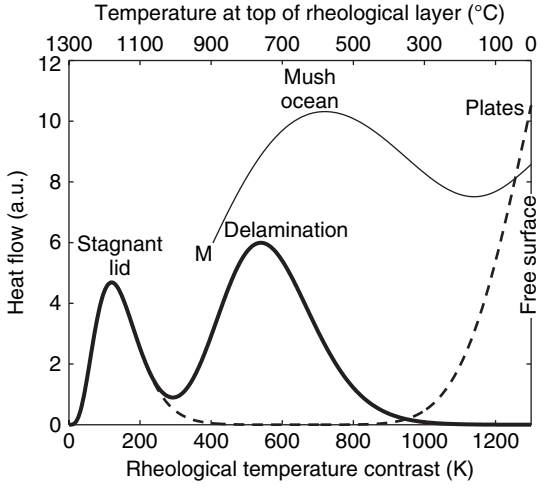

Figure 5 The heat flow in arbitrary units from [19]. The author has adjusted the constant a in each model so that the amplitude of the peaks is comparable for schematic plotting convenience. The second peak of the solid curve corresponds to delamination of the lithosphere, $n = 8$. The dashed curve represents plate tectonics. The computed heat flow is still increasing when the rheological temperature contrast is equal to its maximum possible value, the difference between the asthenosphere and the free surface. This defines a maximum. The author represents a plastic rheology with $n = 24 (T_\eta = 50\,\text{K})$. The (top) scale for temperature at the top of the rheological boundary layer applies to the present Earth. The mush-ocean curve (thin solid line) is purely schematic and applies when the interior of the Earth was much hotter than today. The author draws the curve with weak dependence of heat flow on rheological temperature contrast. No stagnant-lid branch exists; the temperature contrast cannot be lower than that between upwelling mantle and nearly frozen mush (point M).

active boundary layer thickness ΔZ_{rheo} dimensionally:

$$V = \varepsilon' \Delta T_{\text{rheo}} \left[\frac{\partial T}{\partial Z}\right]^{-1} = T_{\text{rheo}} \frac{1}{T'\eta} \left[\left(\frac{\rho g \alpha \Delta T_{\text{rheo}}^2}{T'}\right) + a\left(\frac{\left(\rho g \alpha \Delta T_{\text{rheo}}^2\right)^n}{T'^n \tau_{\text{ref}}^{n-1}}\right)\right] \quad [18]$$

where $T' \equiv \partial T/\partial Z$ compacts notation. The convective heat flow is dimensionally $\rho C V \Delta T_{\text{rheo}}$. Finally, the uppermost part of the rheologically active boundary layer must deform for flow to occur. The effective value of viscosity-resisting flow is that where the temperature is about ΔT_{rheo} below that in the underlying half-space. Applying the viscosity equation [15] yields an equation for the convective heat flow

$$q = \rho C \varepsilon' \Delta T_{\text{rheo}}^2 \left[\frac{\partial T}{\partial Z}\right]^{-1} = \Delta T_{\text{rheo}}^2 \frac{\rho C}{T'\eta_0} \left[\left(\frac{\rho g \alpha \Delta T_{\text{rheo}}^2}{T'}\right) + a\left(\frac{\left(\rho g \alpha \Delta T_{\text{rheo}}^2\right)^n}{T'^{\text{n}} \tau_{\text{ref}}^{n-1}}\right)\right] \times \exp\left[\frac{-\Delta T_{\text{rheo}}}{T_\eta}\right] \quad [19]$$

where η_0 is the viscosity of the underlying half-space. The expression is at a maximum when $\partial q/\partial T_{\text{rheo}} = 0$. We recover results for power-law rheology by retaining only the a term in [19]. One recovers the $n+1$ dependence in [14]; the factor 1.2 is obtained from experiments. One obtains [13] with the $1/(\text{n}+2)$ exponent by setting the convective heat flow in [19] equal to the conductive heat flow $q = k\partial T/\partial Z$ and solving for the temperature gradient.

For application to the Earth, two maxima occur in [19] if the first term dominates at small stresses and small values of the rheological temperature contrast (**Figure 5**). The first maximum represents stagnant-lid convection within a fluid with linear rheology. The second high-stress maximum might represent other situations.

Figure 5 shows a case where the second maximum is within the lithosphere. This represents conditions for delamination of the base of the lithosphere. Ordinarily, the stagnant-lid mode is stable. From [17], its small rheological temperature contrast ΔT_{rheo} implies stresses that are much less than those of the delamination mode. As the rate of nonlinear creep depends on the rheological temperature contrast raised to a high power the upper part of the lithosphere stays rigid.

Delamination requires a large stress perturbation scaling to the stress implied by its ΔT_{rheo} in [17]. In the Earth, this stress could arise from the impingement of a mantle plume, continental collision, low-angle subduction, or continental breakup.

The upper boundary condition on the lithospheric mantle affects delamination. In particular, the hot base of over-thickened continental crust acts as a free surface (Appendix 2). In terms of the heat-flow equation [13], the dimensionless constant A_n is larger for a free surface boundary than a rigid boundary. In terms of [18], the flow velocity is higher if the upper boundary slips freely than if this boundary is rigid. With regard to **Figure 5**, the presence of fluid continental crust affects delamination if the temperature at its base is within the delamination maximum.

Plates are rheological boundary layers extending all the way to the free surface of the Earth. The rheological temperature contrast is thus the full temperature contrast across the lithosphere. On the Earth, existing plate tectonics maintains the high stresses needed to nucleate new plate boundaries as old ones are consumed by continental and ridge–trench collisions. The plate tectonic maximum in **Figure 5** is the intersection of the heat-flow curve with the temperature of the free surface. The author's statements about the transition of stagnant-lid convection to delamination also apply to its transition to plates. Stagnant-lid convection may not produce large stresses in a one-plate planet, making transition to plate tectonics difficult. There is no evidence of it occurring in the geological records of the planets we have observed. However, Solomatov (2004) shows with dimensional and numerical models that this transition may occur under realistic situations.

The transition of mush ocean to plate tectonics is also relevant to the Earth (Appendix 2). **Figure 5** illustrates a time when the Earth's interior was hot enough to maintain a mush ocean. As drawn, maxima correspond to mush-ocean convection where the base of basaltic crust founders and plate motion where the entire crust founders. The rheological temperature contrast is greater than the contrast between solid upwelling mantle and nearly frozen mush. The heat flow is weakly dependent on the rheological temperature contrast. The mush ocean may have behaved as a mixture of these modes.

9.06.2.5 Pressure-Release Melting at Mid-Oceanic Ridges

Upwelling mantle melts beneath mid-oceanic ridges. The melt ascends and freezes to form the basaltic oceanic crust. Both the basaltic crust and the depleted

residual mantle are less dense than the melt-source region from which they differentiated. These density changes are large enough to affect plate dynamics. Lithosphere formed from hot mantle is hard to subduct (e.g., Sleep and Windley, 1982; Davies, 1992; van Thienen *et al.*, 2004).

Following Klein and Langmuir (1987), McKenzie and Bickle (1988), Plank and Langmuir (1992), and Klein (2003), we present a short discussion of how this process affects plate motion. Crudely, the Earth's mantle consists of olivine, orthopyroxene, clinopyroxene, and an alumina-bearing phase. Garnet, a dense mineral, bears the Al_2O_3 at mantle depths below ~100 km. At crustal depths, low-density feldspar contains most of the Al_2O_3. Mid-oceanic ridge basalt that has a near surface density of ~3000 kg m^{-3} is eclogite below 150- km depth at the interior temperature of the mantle with a density of 3600 kg m^{-3} at current plume temperatures (Sobolev *et al.*, 2005). The stability field of eclogite is temperature dependent; subducted basalt begins to form eclogite at ~30 km depth. The density difference of basalt with respect to eclogite is significant. For comparison, the volume thermal contraction coefficient of mantle is 3×10^{-5} K^{-1}; a temperature change of 1000 K produces a density change of only ~100 kg m^{-3}.

Melting occurs as pressure decreases within the mantle upwelling beneath ridges. Eutectic melting illustrates the mass balance at low melt fractions although it is an inadequate representation of melt chemistry. In addition, clinopyroxene and the alumina-bearing phase are exhausted before olivine and orthopyroxene; further temperature increases after ~50% melting result in modest amounts of additional melting.

For additional simplicity we let the melting temperature be a linear function of depth:

$$T_m = T_0 + \beta Z \quad [20]$$

where T_0 is the melting temperature at the surface and β is the gradient of melting temperature with depth Z. The temperature of the upwelling material in the absence of melting is

$$T_a = T_p + \gamma Z \quad [21]$$

where T_p is potential temperature and γ is the adiabatic gradient. Melting begins at the depth where the curves intersect:

$$Z_m = \frac{T_p - T_0}{\beta - \gamma} \quad [22]$$

The temperature above this depth lies on the melting curve. The specific heat for cooling the material from the solid adiabat equals the latent heat for partial melting:

$$\rho C(T_a - T_m) = LM \quad [23]$$

where L is the latent heat per volume and M is the fraction of partial melt. Solving for the fraction of melt gives

$$M = \frac{\rho C}{L}\left[T_p - T_0 - (\beta - \gamma)Z\right] \quad [24]$$

The total thickness of melt production is crudely that in a column that reaches the surface

$$\Phi = \int_0^Z M \, dZ = \frac{\rho C\left(T_p - T_0\right)^2}{2L(\beta - \gamma)} \quad [25]$$

The actual mantle is not precisely eutectic. The heat-balance equation becomes

$$\rho C(T_a - T_m(M, Z)) = LM \quad [26]$$

where the melting temperature is a function of depth and fraction of melt. One solves [26] numerically and integrates the fraction of melt upward (as $M/(1-M)$ to correct geometrically for compaction of the matrix). For a ridge axis, the computed thickness of melt equals the depth to the base of the crust. One truncates the integral at that depth. One truncates at the base of the lithosphere for mid-plate melting.

We calibrate the eutectic model for quick calculations so that it represents melt fractions for the actual melting in the present Earth, $(\beta - \gamma)$ is 3.2 K km^{-1} and $L/\rho C$ is about 840 K. The depth of extensive melting Z_m is 56 km. These parameters give 6 km of average oceanic crust. The temperature change per thickness of crust is

$$\frac{\partial T_p}{\partial \Phi} = \frac{L(\beta - \gamma)}{\rho C(T_p - T_0)} = \frac{L}{\rho C Z_m} \quad [27]$$

This expression yields the expected value of 15 K km^{-1}.

These considerations imply that oceanic crust was much thicker in the past when the interior of the Earth was hotter (**Figure 6**). Consider a time in the past when the mantle was 200 K hotter than now. The oceanic crust was ~14 km thicker than now or 20 km thick. It everywhere resembled the thick hot-spot crust beneath Iceland. This buoyant crust did not easily subduct until cooling had progressed downward into the mantle lithosphere. Present-day oceanic crust, such as remnants of the Farallon

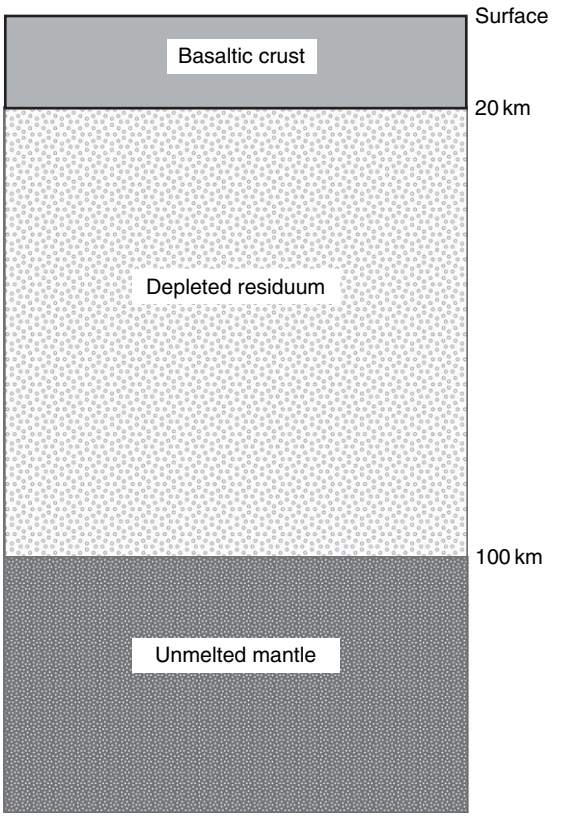

Figure 6 Section through oceanic lithosphere where upwelling mantle starts melting at 100 km depth. This lithosphere is difficult to subduct. Both the crust and depleted residuum are buoyant relative to the underlying mantle. Unlike basaltic mush, the depleted residuum is quite viscous and does not internally convect.

Plate (Atwater, 1970; Wilson *et al.*, 2005), became difficult to subduct at 5–10 My age. As cooling time depends on the square of the depth, 20-km-thick crust would be difficult to subduct at $(20/6)^2 = 11$ times these ages or 55–110 My.

Plate tectonics was even less efficient in subducting thicker crust when the mantle was hotter than in the example. This implies that convection within the partially molten mush carried heat to the surface. We consider this epoch in the next section. Davies (Chapter 4.23) discusses an alternative hypothesis for efficient plate tectonic on early Earth. The basaltic component separated from the olivine-rich and accumulated at the base of the mantle. During this epoch, the oceanic crust was much thinner than that in the author's discussion that assumes that the major element composition of the mantle rising at midoceanic ridges did not vary over time.

9.06.3 Aftermath of the Moon-Forming Impact

The violent birth of the present Earth makes for simple physics (Sleep *et al.*, 2001; *see* Chapters 9.04 and 9.01). A Mars-sized body collided with a Venus-sized body at ~4.5 Ga, leaving the Earth–Moon system. The core of the projectile merged with the target's core. Most of new Earth's mantle was hot enough to vaporize at upper-mantle pressures. The vapor radiated heat, quickly forming silicate cloud tops at ~2300 K. The photosphere radiated at this temperature for ~2000 years. During this time, all mantle material circulated through the cloud tops. The Earth lost far more heat during this epoch than during its subsequent history. At the end of this epoch, material arriving at the surface was mostly molten and silicate clouds were only a transient local phenomenon. In the next few 100 years, surface regions cooled so that some solidification occurred around 2000 K. A global solid crust formed at ~1500 K. The water and CO_2 atmosphere then became opaque. The surface heat flow dropped to that of a runaway greenhouse, ~150 W m^{-2}, enough to freeze the mantle and cool it by a few hundred kelvins in a couple of million years. Tidal dissipation from the Moon prolonged this interval by over 3 million years (Zahnle *et al.*, 2007). Thereafter, sunlight and the concentration of greenhouse gases controlled climate with liquid water at the surface. A modest ~200°C surface greenhouse may have persisted until carbonate formation and crustal overturn sequestered the CO_2 in the subsurface.

Asteroids bombarded the early Earth. The precise timing of the impacts is unclear. Current lunar data are compatible with a relatively quiescent period from 4.4 to 4.0 Ga followed by 'late heavy bombardment' between 3.8 and 4.0 Ga (see Ryder (2002), Zahnle and Sleep (2006), Zahnle *et al.* (2007)). Extrapolating from the Moon constrains the size and total number of objects that hit the Earth. Over 100 of them were greater than 100 km in diameter. About 16 were larger than the largest (200 km diameter) object that hit the Moon. A few (0–4) may have been big enough (>300 km diameter) to boil the ocean to the point that only thermophile organisms survived in the subsurface. These impacts on Earth brought brief returns of rock vapor and steam greenhouses.

The effect of impact effect on tectonics, however, was modest. The Moon, which was subjected to the

same bombardment, retains its upper crust over much of its surface. Cavosie *et al.* (2004) saw no evidence of impacts in their sample of detrital zircons going back to ~4.4 Ga. This includes zircons with metamorphic rims, which might show annealed shock features. Conversely, the durations of the rock vapor atmosphere and the hot greenhouse were geologically brief and unlikely to preserve rocks. The existence of 4.4 Ga detrital zircons and ~4.5 Ga continent-like geochemical reservoirs (Harrison *et al.*, 2005) do not bear on the reality of these epochs.

9.06.3.1 Early Mush Ocean

The liquid magma ocean ended about the same time that the surface froze (Sleep *et al.*, 2001; Zahnle *et al.*, 2007; *see also* Chapters 9.04 and 9.01). Modern fast ridge axes provide analogy. Magma entering the axis freezes quickly (Sinton and Detrick, 1992). The bulk of the 'magma' chamber is mostly crystalline mush. Only a thin (tens of meters) lens of fully molten rock exists at the axis.

These observations show that molten mafic bodies quickly freeze to mush. They provide quantification on the rate that liquid convection within the chamber delivers heat to the surface. The parametrized convection equation [8] for a linear rheology of basaltic melt applies. Current ridge axes provide a minimum estimate for the convective heat flow from the liquid magma ocean. Molten material of mantle composition is orders of magnitude less viscous than modern basalt (Liebske *et al.*, 2005).

Estimating the heat flow through a modern magma lens at the ridge axes driven by latent heat is straightforward. We balance the heat per time per length of ridge with the heat flow per length of ridge axis out of the width of the magma lens. This yields that

$$q = \frac{L Z_c v}{W} \qquad [28]$$

where $L = \sim 1.5 \times 10^9\,\mathrm{J\,m^{-3}}$ is the latent heat of freezing, W is the width of the magma lens, Z_c is magma chamber thickness, and v is the full spreading rate (Sleep *et al.*, 2001). The fastest spreading centers have the highest heat flow. We retain parameters from the work of Sleep *et al.* (2001). The highest full spreading rate on the modern Earth is $155\,\mathrm{mm\,yr^{-1}}$, magma chamber thickness is ~5 km, and the lens width is 1 km. These quantities yield a heat flow of $40\,\mathrm{W\,m^{-2}}$. The latent heat of the entire mantle could maintain this heat flow only 3 My.

This implies that the fully molten magma ocean was short-lived on the Earth. The fully molten ocean could well have cooled to mush during the runaway greenhouse. At the time the magma ocean froze to mush, it was only a few hundred kelvin hotter than the modern mantle. This fossil heat and radioactivity drove tectonics for the subsequent ~4.5 billion years.

Like a modern ridge axis, convection in the underlying solid mantle limited heat transfer through the mush ocean. This process has many aspects of stagnant-lid convection (Appendix 2). The viscosity of the solid mantle changes greatly with cooling, controlling the vigor of convection. However, magma from the underlying solid convection sees the floor of the mush chamber as a nearly fluid permeable interface. The multiplicative constant in [9] is thus larger than the multiplicative constant for convection beneath a rigid stagnant lid. The relevant temperature difference driving convection in [9] scales to the difference between the liquidus and the solidus. This quantity decreased modestly as the mush ocean cooled. The crustal lid of the mush ocean foundered and deformed, grossly like plates.

The heat-balance equation [1], the convection equation [9], and the strong dependence of viscosity on temperature [12] imply quick cooling at high temperature and low viscosity followed by slower cooling (**Figure 3**). The Earth transitions from its earliest history where radioactive heat generation is a trivial item in the heat budget to the present status where radioactive heat generation is in crude steady state with surface heat flow.

9.06.3.2 Steady-State Mush Ocean and Transition to Plate Tectonics

As noted in Section 9.06.2.1, radioactive heat generation in the Late Hadean was comparable to the modern global average heat flow $\sim 0.07\,\mathrm{W\,m^{-2}}$. In the models, the heat flow is $\sim 0.13\,\mathrm{W\,m^{-2}}$ at 4.0 Ga. Global tectonic rates of $(0.13/0.7)^2 = 3.4$ times present could have vented this heat. This radioactive heat production is low enough to permit a significant hiatus in tectonic vigor at the time of transition between the mush ocean and plates. The radioactive heat generation would increase mantle temperature ~42 K in 100 My in the absence of heat flow from the core and out of the surface. For example, a total hiatus of 250 My would warm the mantle by only 100 K.

In terms of eqn [1], the heat flow and the interior temperature need not have decreased monotonically with time (Sleep, 2000; Stevenson, 2003). The surface heat flow as a function of temperature may be multivalued, here with branches for plate tectonics and mush ocean (**Figure 1**). The mush ocean could well have overcooled the mantle (**Figures 2** and **3**). Hot buoyant material rose to the top of the mantle, cooling near the surface of the mush ocean. The cooled material foundered, eventually filling the mantle from bottom up. The mush ocean ceased when the cooled material filled the mantle (point A to point B, **Figure 1**). Sluggish subsequent plate tectonics persisted for several hundred million years until radioactivity heated up the mantle enough to restart the mush ocean (point C to point D). The heat flow and interior temperature looped over points ABCD until the heat flow from plates (point B) was less than radioactive heat generation.

As noted below, the brief mush-ocean episodes could be periods of rapid continent generation because hydrated crust subducts into basaltic mush. The ascending water causes the mush to melt extensively producing a granitic (*sensu latu*) magma.

An alternative possibility is that the mush ocean transitioned monotonically to sluggish plate motions inhibited by thick oceanic crust as discussed in Section 9.06.2.5 (Korenaga, 2006). Plate rates were slower than present. Mush ocean and plates prevailed in different regions. The mantle temperature remained at the transition (**Figure 3**) and the heat flow remained between the plate and mush-ocean values (**Figure 2**). Eventually, radioactive heat production decreased to where plate tectonics could vent it. Plate tectonics thereafter cooled the Earth.

The transition as drawn is discontinuous. Any strong dependence of global heat flow on interior temperature will trap the mode of convection in transition until radioactive heating wanes enough to be balanced by the less-vigorous mode. In the early days of plate tectonics, it was thought that the dependence of heat flow on interior temperature was so strong that the Earth achieved its present interior temperature soon after it accreted (Tozer, 1970). This concept applies in the monotonic model over much of the early history of the Earth, though not now.

We apply Section 9.06.2.5 to put the above heat balance inferences into a petrological context. Conditions for maintaining the mush ocean in steady state are relevant to the causes of the mush ocean's eventual demise. The mush ocean consists of a frozen crust with some continental material, melt lens where ascending magma ponds and freezes to mush, a thick layer of mush, and the underlying mantle (**Figure 7**). As already noted, solid-state convection in the mantle limits the rate of heat transfer (Appendix 2).

The base of the mush acts as a permeable interface. Ascending mantle melts. Dikes ascend through the mush and into a magma lens. Some of the magma freezes to mush. Some freezes to form basaltic crust. The crustal volume stays in steady state; cool thick regions of the crust founder into the mush in a process like subduction. The dense base of the mush and foundered crust sink into the mantle, balancing the magmas injected from the mantle.

We focus on the requirement that the supply of melt equals the return of melt to the mantle. Both processes depend on the temperature of the upwelling mantle. If the mantle is hot enough, the thickness of the mush lens self-organizes to a steady state.

First the frozen mush at the base of the ocean needs to be dense enough that it sinks into the mantle. Early in the Earth's history, the mantle was hot enough that upwelling material melted completely. The melt composition hence was mantle composition. Cool material was denser than hot material. Mush sank once frozen.

Later on, the mantle cooled to a temperature where basalt was the most voluminous melt. The cooled basaltic crust has about the same composition as the underlying mush. It can subduct and founder into the mush ocean. However, as already noted, basaltic material and its depleted residuum are less dense than unmelted mantle at shallow depths. However, the dense mineral garnet makes basaltic composition heavier below ~150 km depth. (Sobolev *et al.* (2005) discuss melting of the ecologite component in plumes.) The base of the mush ocean sinks into the mantle if it is deeper than that depth, but not if it is shallower. This feature tends to prevent the base from getting deeper than ~150 km depth.

Second, the balance between recharge from basalt from the upwelling mantle and subduction of slabs into the mantle determines whether the mush chamber thickens or thins. The models assume that the chamber (in the plate mode) thickens once the mantle becomes hotter than 1600°C, the potential temperature where significant melting starts at 150 km depth in [22]. The melt flux needs only to replenish the basaltic material that sinks back into the mantle. It does not have to be hot enough to generate a 150 km thickness of melt in [25].

From this reasoning, the mush chamber becomes unstable to depletion once the mantle temperature

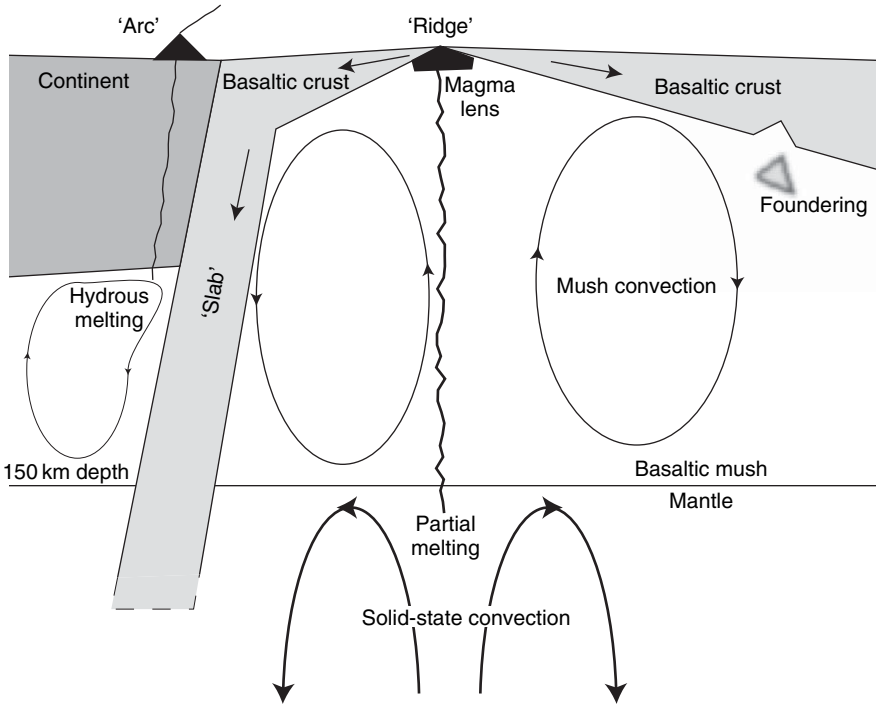

Figure 7 Schematic diagram of mush ocean with vertical exaggeration. Analogs to plate tectonic features are in quotes. Upwelling mantle partially melts. Melt ascends into the magma lens at the ridge axis and freezes, making basaltic crust and basaltic mush. Basaltic crust both subducts as slabs and founders as blocks. Partial melting of hydrated basalt produces arcs and continents. Convection within the mush transfers additional heat from the mantle. Slabs, entrained mush, and foundered blocks return basaltic material to the mantle. Thick lithosphere composed of depleted mantle residuum stabilized some continental regions (not shown).

drops below that needed for recharge. The rounded potential temperature where this happens in the models is 1500°C, where melting in [22] begins at 118 km depth. In the nonmonotonic model (**Figure 1**), convection jumps to plate tectonics. The remaining mush freezes to lithosphere and the foundering regions of crust become slabs. At this time, the ascending mantle generates only 20 km of oceanic crust in the linearized model (**Figure 6**). This is thick enough that plate tectonics cannot vent the heat generated by radioactivity (**Figure 2**). The mantle heats up until enough ascending material melts for the mush ocean to restart (**Figure 3**).

Alternatively, as in the monotonic model, convection becomes sluggish with only local and transient regions of mush ocean, as the mantle approaches the critical temperature to maintain the mush ocean. The convective heat flux balances radioactive heat generation during a long transition period that lasts until after the end of the Archean.

It is obvious that the mush ocean as envisioned provides an efficient mechanism for generating continental crust at arcs. Water from the slab enters hot gabbroic mush, rather than mantle peridotite in standard subduction. The melt is granitic (*sensu latu*). Its detailed geochemistry is beyond the scope of this chapter.

9.06.3.3 Zircon Evidence

As discussed in the last section, Earth scientists know too little about the material properties of the Earth to make a more quantitative prediction of the vigor of a mush ocean or the timing of its demise. The crust of Mars may provide some analogy with future exploration. Right now the mush ocean is the first epoch of Earth's interior with even a meager geological record. Geochemists have extracted detrital zircon crystals from Archean and Proterozoic quartzites in Australia (e.g., Cavosie *et al.*, 2004; Dunn *et al.*, 2005). The igneous ages of oldest crystals are ~4.4 Ga, a time when the mush ocean might have persisted. The old zircons resemble those from modern granites (*sensu latu*) (Cavosie *et al.*, 2004; and references therein). In

particular, some of the granites formed at the expense of sediments derived from meteoric weathering.

Isotopic studies of 4.01–4.37 Ga zircons provide evidence of an older separation of the parent element Lu from the daughter element Hf in the Earth's interior. Within the resolution of a few million years after the moon-forming impact, fractionated continental-type crust with elevated Lu/Hf covered part of the Earth's surface (Harrison *et al.*, 2005). Its depleted low-Lu/Hf complement comprised a significant mantle reservoir.

These data imply some form of crustal overturn analogous to modern subduction. Hydrous mafic rocks either melted directly or dehydrated causing the surrounding hot mush to partially melt. The surface needed to be cool enough for liquid water; a warm greenhouse at ~200°C suffices as hydrous minerals are stable at black-smoker temperatures of 350°C. The hydrated rocks needed to founder. Getting buried by subsequent lava flows or more traditional subduction suffices. They then needed to be heated, no problem given a mush ocean; that is, the typical magmatic rocks associated with subduction are not strong indications of the modern process, especially when they are out of context in detrital zircons.

Cavosie *et al.* (2004) present a constraint on the vigor of crustal recycling processes after 4.4 Ga. Age gaps and clusters exist within their sample suite, just like with a modern orogenic belt (**Figure 8**). If further sampling confirms this finding, terrane-scale regions experienced tens of million-year periods of quiescence. This extends the result of Burke and Kidd (1978) that the base of Archean continental crust did not undergo continuous melting to form granites into deep time. Thermally at ~4.4 Ga, mantle lithosphere existed at least locally beneath continent-like crust. This is consistent with a sluggish mush ocean or with plate tectonics. There is no evidence of any global hiatus in tectonic vigor.

The gaps between events between 4.4 and 3.8 Ga are 50–100 My compared with 500–1000 My for the subsequent history, including modern zircon suites. Taken at face value, crustal recycling rates were ~10 times the present. Sleep and Zahnle (2001), for example, used this rate for modeling Hadean geochemical cycles. The heat flow was ~3 times the present (0.21 W m^{-2}) implying a cooling rate of 280 K per billion year for the radioactive heat generation used above. The lithosphere from [3] was about 40 km thick, enough in analogy to the modern Earth to have plate-like characteristics. This cooling rate is about the limit that could be sustained over 2 billion years until the end of the Archean with the available heat. As already noted, much of the heat probably came out early when the interior was still quite hot.

Alternatively, the gaps and clustering in the ancient zircon suites are analogous with those that exist today on an active continental margin. In this case, the ancient and modern gaps are similar, tens of million years. The crustal sources of the Hadean zircons formed within tectonically active areas. It took time for there to be enough continental crust that stable continental interiors were kinematically

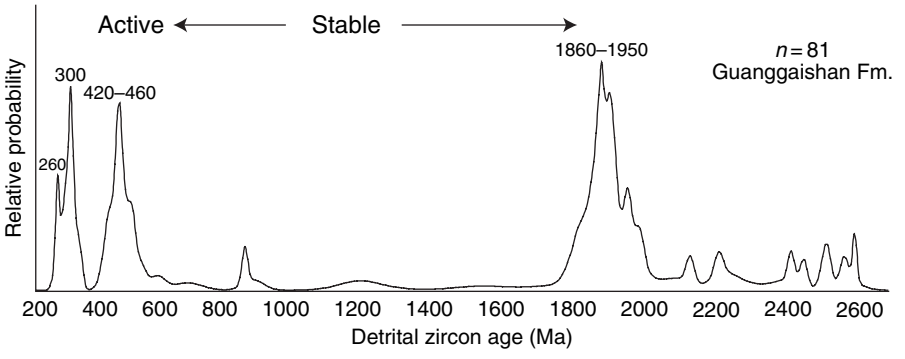

Figure 8 Age distribution of detrital zircons from the Guanggaishan formation of Ladianian (Triassic) age in eastern China illustrates problems in obtaining the age of Hadean tectonics from ancient populations. The sample of 81 ages resolves four peaks. The source region was active before the deposition age of ~228 Ma and stable for a billion-year interval before then. It is not known whether Hadean source regions represent the relatively stable or the relatively active regions at that time. It is inappropriate to infer global events from this Chinese locality and quite premature to infer global events from a few zircon populations from the early Earth. Data from Weislogel AL, Graham SA, Chang EZ, Wooden JL, Gehrels GE, and Yang H (2006) Detrital zircon provenance of the Late Triassic Songpan - Ganzi complex: Sedimentary record of collision of the North and South China blocks. *Geology* 34(2): 97–100.

possible. In any case, tectonics after 4.4 Ga were sluggish enough that some Hadean continental crust survived to at least the end of the Archean.

9.06.4 Dawn of Plate Tectonics

It is not clear when modern plate tectonics started. We see none of the Earth's original crust and when we do get zircon samples at ~4.4 Ga, the evidence is compatible with plate-like processes. We see no evidence for any period where the surface of the Earth was a one-plate planet like Mars. The viable candidates are a mush ocean with significant regions of continental crust and lithosphere and plate tectonics with solid lithosphere above solid mantle. As noted already, the transition between these two modes may have well been protracted, regional, and gradual. Various aspects of modern tectonics may have begun at different times.

The widespread occurrence of vertical tectonics in the Archean does not preclude plate processes. The author's discussion follows comments by Sleep (2005) and Condie and Benn (2006). As already noted, vertical tectonics occur over broad swaths of the present Earth. Second, the Earth's interior was obviously hotter in the Archean than at present. Volcanic sequences tended to be thicker and the granitic crust was more easily mobilized by mafic and ultramafic intrusions. It is likely that some continental areas, like the Minto province in Canada, formed from remobilized oceanic plateaus (Bédard *et al.*, 2003). Alternatively, the Minto basaltic lithosphere may be a remnant of a mush-ocean plate.

Van Kranendonk *et al.* (2004) discuss the eastern Pilbara craton. A prolonged period of crustal formation occurred from 3.47 to 3.24 Ga. Notably supracrustal rocks on the domes are not extensively metamorphosed. This indicates that the surrounding greenstone belts subsided and that the tops of the domes were never deeply buried. It is incompatible with assemblage as a series of alpine-style thrust sheets. An analogous situation exists in the 2.7 Ga Belingwe Belt in Zimbabwe. Sediments on the flanks of the belt are weakly metamorphosed (Grassineau *et al.*, 2005). This is evidence that the center of the belt subsided *in situ* without deeply burying its flanks. It is evidence against this greenstone belt being a 6-km-thick allochthonous oceanic plateau as proposed by Hofmann and Kusky (2004).

Careful work indicates that horizontal tectonics and vertical tectonics coexisted in the Archean. Hickman (2004) shows that vertical tectonics prevailed in the eastern Pilbara craton before 2.9 Ga, while horizontal tectonics are evident in the western Pilbara craton. Lin (2005) demonstrated the formation of a greenstone belt as the keel of a strike-slip deformation zone in the Superior Province.

We continue by reviewing evidence for the earliest documentation of various plate tectonic features. To do this, we need to consider both preservation bias and mechanics. Overall, we see plate-like features as soon as we have a record that could reasonably provide them.

9.06.4.1 Seafloor Spreading and Oceanic Crust

Almost all oceanic crust eventually subducts into the mantle. The tidbit that survives provides a biased sample. Parautochthonous ophiolites from back-arc, forearc, and breakup margins start adjacent to continental crust. These rocks may well show continental chemical affinities (Hofmann and Kusky, 2004). Thin oceanic crust formed during cool slow breakups is most likely to stay intact. Conversely, we are not likely to find intact 'normal' Archean oceanic crust if it was in fact as thick as modern oceanic plateau crust (Moores, 2002; Condie and Benn, 2006).

To bring up another uncertainty, mafic rocks formed away from ridge axes mimic ophiolites in tectonically disrupted exposures. The rift zones of major edifices like Hawaii constitute a serious problem. The rifts spread at a few centimeters per year. In a submarine section, pillow basalts overlie dikes and then gabbro (e.g., Okubo *et al.*, 1997). Subaerial pahoehoe may even be difficult to distinguish from submarine pillows at highly deformed and metamorphosed outcrops. Cover tectonics on the flanks of edifices resemble foreland thrusts when viewed locally (e.g., Morgan *et al.*, 2003).

There are certainly abundant pillow basalts and other mafic and ultramafic rocks in the Archean. Moores (2002) reviews candidates for oceanic crust. The oldest putative ophiolite is the 2.5 Ga Dongwanzi complex in China (Kusky *et al.*, 2001). Too little is known to appraise this claim. Fumes *et al.* (2007) pillow basalts, sheet dikes, and gabbros from the 3.8 Ga Issua belt in southwestern Greenland. As with many modern ophiolites, these rocks show arc affinity. This exposure suffices to show that sea-spreading and ridge-axis hydrothermal circulation occurred on the early Earth. However, these rocks provide little constraint on the thickness

of ancient oceanic crust as the base of the ophiolite is not exposed.

Blocks of apparent oceanic crust in the Pilbara block are better studied and are older >3.2 Ga candidates (Hickman, 2004; Van Kranendonk *et al.*, 2004). Upper-crustal rocks at Marble Bar are well preserved, providing an early 3.46 Ga example of carbonate formation by deep marine hydrothermal fluids (Nakamura and Kato, 2004). Kitijima *et al.* (2001) studied similar nearby 3.46 Ga oceanic basalts at North Pole, Australia. Using boiling relationships, they obtained that the water depth was comparable to modern ridge axes with a best estimate of 1600 m.

Abyssal peridotites distinguish conventional oceanic lithosphere from lithosphere formed in a mush ocean. This rock type occurs as soon as there is geological record at 3.8 Ga in Greenland (Friend *et al.*, 2002). However, younger examples are not described until the end of the Archean, for example, as part of a putative ophiolite in China (Kusky *et al.*, 2001). This dearth might indicate that conventional oceanic lithosphere was uncommon in the Archean. It might indicate the geometrical difficulties of tectonically exhuming the base of thick oceanic crust. There are cumulate ultramafics in the Archean (e.g., Friend *et al.*, 2002; Furnes *et al.*, 2007) so poor preservation potential once emplaced does not seem likely. There is cause for concern about reporting biases, including lack of recognition, lack of study, and publication in ways not retrievable by online search.

9.06.4.2 Transform Faults

The strike-slip motion on transform faults obviously dissipates energy but provides no gravitational driving force (Sleep, 1992). Mathematically, strike slip is toroidal motion around a vertical axis. Such motion cannot occur unless rheology is strongly laterally heterogeneous, that is, rigid plates and weak plate boundaries. Polat and Kerrich (2006) summarize known Archean strike-slip faults. We have already noted the difficulty of recognizing strike-slip motion in the presence of associated vertical tectonics (Chen *et al.*, 2001; Lin, 2005).

Continental margin transform faults preserve a record of oceanic tectonics on their outboard sides (Sleep, 1992). Their length provides a minimum limit of plate size. The duration of sense of slip constrains the ratio of plate size and plate velocity. One could get the relative plate velocity directly with piercing points or with the demise of volcanism as a Mendocino-type triple junction passed. The gross endeavor may be feasible. Atwater (1970) applied these tectonic concepts to explain Tertiary California geology. There are limits to resolution. Coastal California is quite complicated when examined in detail (Wilson *et al.*, 2005).

The Inyoka Fault in southern Africa is the oldest 3.2 Ga well-preserved example. It cuts syntectonic basins of the Moodies group (Huebeck and Lowe, 1994; de Ronde and de Wit, 1994). Like the San Andreas Fault, motion is parallel to the gross strike, piercing points are not recognized in spite of detailed mapping (de Ronde and de Wit, 1994; de Ronde and Kamo, 2000). Motion is associated with detachment faulting (Huebeck and Lowe, 1994; Kisters *et al.*, 2003).

9.06.4.3 Subduction and Continental Lithosphere

We have already noted that igneous rocks analogous to arc magmas are ubiquitous back to the time ~4.5 Ga of the first hint of a geological record (Harrison *et al.*, 2005; Polat and Kerrich, 2006). We have also noted that foundered crust within a mush ocean is likely to be analogous to the crust in modern slabs. Thrusting and rifting are likely to resemble the modern analog at shallow depths of exhumation as brittle failure is involved. On the other hand, Stern (2005) contends that the lack of high-pressure and ultrahigh-pressure metamorphism on the ancient Earth indicates that modern subduction did not occur.

Subduction, however, merely requires that surface rocks penetrate to great depth, while ultrahigh metamorphism requires that these rocks return to the surface in a recognizable form. The higher temperature in the Archean mantle clearly heated subducted material. Any subducted material that made it back to the surface was likely to be hotter than modern returning material (Condie and Benn, 2006).

We journey downward into deep cratonal lithosphere in search of a better rock record. Lithospheric mantle beneath cratons is less dense than normal mantle. This along with its higher viscosity keeps continental lithosphere from being entrained into the deeper mantle by stagnant-lid convection (Doin *et al.*, 1997; Sleep, 2003). Its great yield strength guards it during continental collisions (Lenardic *et al.*, 2003). The oldest in-place diamond pipe is 2.7 Ga in the southern Superior Province of Canada (O'Neill and Wyman, 2006). Detrital diamonds in the

2.5-Ga Witwatersrand sequence also indicate that thick stable Archean lithosphere had already cooled into the diamond stability field by that time (Nisbet, 1991, p. 61).

The Archean subsurface crystallization age of xenoliths in diamond pipes and diamond inclusions is well known. For present purposes, sulfides in ~2.9-Ga diamond inclusions from South Africa studied by Farquhar *et al.* (2002) are relevant. The sulfides have mass-independent sulfur fractionation. This indicates that this sulfur was exposed to UV radiation in an anoxic (<2 ppm O_2) atmosphere (Pavlov and Kasting, 2002). The sediments and altered volcanic rocks containing this sulfur were subducted into the ~200 km-deep lithosphere. This material remained sequestered until tapped by a kimberlite.

In addition, some deep lithospheric samples provide evidence that their depths of formation were shallower than their depths of sequestration (Jacob *et al.*, 2003; Menzies *et al.*, 2003; Saltzer *et al.*, 2001; Schulze *et al.*, 2003a, 2003b; Canil, 2004). This feature and the chemistry of the samples indicate entrainment to depth in the wedge above the slab. Conversely, they do not require highly elevated temperatures that would generate komatiites and their residuum at ~200 km depth.

9.06.5 The Rate of Plate Tectonics over Time

The record after 3 Ga becomes increasing interpretable in terms of the rates of plate motions. One would like to deduce the change in the temperature of the Earth's interior over time along with the variation in the evolution of plate motions. In the absence of magnetic lineations, methods grab at straws.

One approach utilizes the longevity of geological features. This has already been discussed in Section 9.06.3.3 with the clusters and gaps in detrital zircon population ages. Application of this method becomes simpler after 3 Ga in that one can more easily ascribe a tectonic process to an age. The length of the Wilson cycle between passive margin breakup, to arc collision, and final continental collision is attractive. The interval between supercontinent assemblies is a more macroscopic aspect. Mention has already been made to the duration of strike-slip events on active margins. The formation-to-accretion duration of seamounts and the ridge-to-trench lifetime of ophiolites provide direct information on oceanic plates (Moores, 2002).

Korenaga (2006) briefly reviewed this evidence. Additional data since Sleep (1992) discussed tectonic rates have not provided much better constraints. The main difficulty is that plate velocities and the durations of margins, ocean crust, and seamounts are highly variable on the modern Earth. Other than that, rates have not systematically varied by a factor of 2 from current rates over the last 3 Ga; we do not attempt to decipher a trend. We note that Korenaga (2006) contends that rates have actually increased since 3 Ga.

Model-dependent estimates of ancient plate rates come from dynamic considerations. These estimates are coupled with estimates of the interior temperature of the mantle, which we discussed first. There is general agreement that the mantle was hotter at 3 Ga than now. The amount of change is not well resolved. A major difficulty is that the modern source temperature of mantle-derived volcanic rocks is variable, with plume-related material hotter. Taking this into account Abbott *et al.* (1994) and Galer and Mezger (1998) give their preferred temperature decrease of 150 K. A second difficulty is that hydrous magma melts at a lower temperature than anhydrous magma. Grove and Parman (2004) contend that komatiites are hydrous magmas and the mantle was only 100 K hotter. Arndt (2003) notes that this is unlikely with komatiites in general. There has been progress in distinguishing arc from mid-oceanic lavas in the Archean (Polat and Kerrich, 2006). This along with recognition of seamount lavas should help with obtaining a representative source region temperature in the Archean.

Archean cratonal xenoliths provide additional evidence of the temperature in the Archean mantle. Canil (2004) showed that trace elements in his samples are compatible with formation within a subduction zone, but not with formation from a hotter magma at their present lithospheric depth.

The freeboard of the continents provides both a kinematic constraint and a dynamic constraint. Basically, many Archean terranes have never been deeply eroded or deeply buried by sediments once they were stabilized (e.g., Galer and Mezger, 1998). Thus, the elevation of these regions above sea level has not changed much. If the amount of seawater has been relatively constant, the available room in ocean basins determines sea level. Thick Archean crust is more buoyant than modern crust and should cause a sea-level rise. Sea level rises as global continental area increases. Vigorous plate tectonics implies that the oceanic basin is filled with young shallow crust. This causes a sea-level rise. Overall, the data are

compatible with plate rates comparable to present since 3 Ga.

Mechanics provide a more reliable version of this constraint that does not involve ocean volume (England and Bickle, 1984). The initial thickness of Archean continental crust is similar to that of young crust. Continental crust is buoyant and would spread laterally like oil over water if it were fluid. A compressional orogeny must overcome this force to form the continent. The available force scales to the ridge push force in [5] and hence to the age of seafloor at subduction t_E. The lack of change in compressional orogenies since 3 Ga indicates that rate of plate overturn has not changed much.

Paleomagnetic data provide constraints on mainly continental plate velocities. For example, Blake *et al.* (2004) obtained precise radiometric ages on strata in the eastern Pilbara craton for which paleolatitudes had been determined. Samples at 2721 ± 4 Ma and 2718 ± 3 Ma differ by 27° or 3000 km. Taken at face value, the drift rate was 1000 mm yr^{-1}. The drift rate was at least 100 mm yr^{-1} within the error of the data. The faster rate is ~10 times modern rates. Sleep and Windley (1982) hypothesized brief episodes of rapid Archean plate motion when old thick lithosphere subducted into the underlying fluid mantle. Available plate size (here at least 3000 km) ended the rapid drift episodes often by continental collisions. Transient mush oceans would have a similar effect. Such periods of rapid drift (if real) need to be included in the global average plate motion.

9.06.6 Death of Plate Tectonics

We have already shown that the rock vapor atmosphere and the mush ocean ceased when the available energy flux failed to maintain them. Plate tectonics will meet the same fate as the mantle cools. The process, called ridge-lock, involves melt generation at ridge axes. If the interior temperature is lower by 50 K, much less melt is generated, see equation [25]. Solid peridotite rather than a fluid mush chamber and sheet dikes must deform for spreading to occur.

In the model (**Figures 1–3**), the mantle becomes too cool for plate tectonics in the future at −0.9 Ga. The heat flow drops to the stagnant-lid branch (**Figure 1**, point E to point F). The mantle slowly heats up but does not become hot enough to restart plates. At −2 Ga, radioactivity heating is in equilibrium with heat flow. The temperature peaks (**Figure 3**). The mantle cools thereafter without returning to plate tectonics. Alternatively, the transition is gradual. The mantle stays at the transition temperature until radioactive heat generation and heat-flow balance, again at −2 Ga (**Figure 3**).

Two harbingers of doom for plate tectonics exist on the present Earth. First, full spreading rates are less than 20 mm yr^{-1} along the Arctic spreading center. This rate is slow enough that material cools as it ascends, violating the adiabatic ascent assumption in deriving [25]. Much of the crust is serpentinite formed from hydrated peridotite (Dick *et al.*, 2003). Gabbros freeze at depth. The flow then carries them to the surface. The radiometric ages of such rocks can be millions of years older than the nominal age of the seafloor.

Second, the Australian–Antarctic spreading center produces a 'discordance zone' with thin ocean crust and rugged topography. The crustal thickness and the unusually large depth at the ridge axis indicate that the upwelling mantle is cooler than that at normal ridges. Ritzwoller *et al.* (2003) present tomography showing an excess potential temperature of the upwelling mantle of 100 K relative to normal ridge axes. They compile petrological excess temperatures of 60–150 K. Herzberg *et al.* (2007) review the global variation of magma source temperatures.

Both the Arctic ridge and the Australian–Antarctic discordance are modest segments of boundaries between major plates. Forces from the rest of these plates could well supply the additional driving force for spreading. When the Earth's interior has cooled, both slow spreading and cool upwelling will tend to lock the entire length of all ridge boundaries. Neither Mars nor Venus provides a qualitative analogy at the present level of ignorance.

A second more subtle effect is already occurring (Sleep, 2005). Stagnant-lid convection provides heat flow to platform regions where the deep lithosphere is not chemically buoyant. The lithospheric thickness in these regions from [13] has increased as the mantle cooled. It is now similar to that beneath cratons where chemical buoyancy defines the base of the lithosphere. Further cooling of the mantle will bring the rheological boundary layer in [14] below the zone of chemical buoyancy everywhere on the planet. The stagnant-lid versus chemical-lid distinction between platforms and cratons then will cease to exist.

9.06.7 Biological Implications

The minimal requirements for the survival of life, energy sources and habitable temperatures, are

linked. Nonphotosynthetic life couples a Gibbs energy-producing reaction, like methanogenesis, with an energy consuming reaction, like ADP⇒ATP. High temperatures speed reaction rates, making energy-producing kinetically inhibited reactions less available. They tend to cause decomposition of the organic matter within all life forms, both squandering the energy that the organism has gone to great ends to convert into a useful form and trashing its genetic information.

We follow the discussion of Sleep *et al.* (2001) to put the establishment of habitable conditions into a tectonic context. The Earth cooled to a solar greenhouse within several million years after its formation. At first, over 100 bars of CO_2 maintained temperatures above 200°C. Carbonates were stable within a thin rind at the surface. The volume of the rind, however, was too small to take up a sufficient quantity. At some stage (4.44 Ga in the model), global heat flow waned to 1 W m^{-2}. The Earth resembled oceanic crust younger than 1 My, the age t_E in [2] of subduction at that time. The crust was a significant CO_2 sink. Carbonate formation now occurs within the uppermost several 100 m of young oceanic crust. Mass balance indicates that crustal overturn was necessary to sequester the CO_2. Available divalent cations in the uppermost crust could take up only ~1/6 of the global CO_2 inventory. Degassing of foundered crust returned an unknown amount of CO_2 to the surface. With a global resurfacing time of 1 My, 6 My was needed to completely consume the dense CO_2 atmosphere in the absence of any degassing or return flux.

Once the primordial CO_2 was sequestered in the subsurface, ejecta from impacts was an effective CO_2 sink. The climate was freezing until life produced methane, a potent greenhouse gas (Sleep and Zahnle, 2001). Life could well have arrived within Mars rocks. Mars was habitable up to 100 My before the Earth. Martian origin is more testable than Earth origin. The Mars record is intact, just hard to retrieve.

After the demise of the thick CO_2 atmosphere, the Earth was habitable except for brief (10^4 years) periods after asteroid impacts (Sleep and Zahnle, 1998; Zahnle and Sleep, 2006; Zahnle *et al.*, 2007). A few impacts large enough to vaporize much of the ocean are likely. They left only thermophile survivors below 1 km deep in the subsurface. Terrestrial life could well root in these survivors.

The main safety requirement is that multiple areas with thermal gradients less than 100 K km^{-1} existed on the planet. For a hard-rock conductivity of 2.4 W m^{-1} K^{-1}, this requires a heat flow less than 0.24 W m^{-2}. This is the heat flow within older oceanic crust when the average heat flow is 0.48 W m^{-2}, occurring at 4.37 Ga in the model. Continent-like regions, however, date from ~4.5 Ga. These low heat-flow regions could well have provided earlier refugia.

Life placed less onerous conditions on tectonics over the next 4 billion years. It mainly demanded that tectonics recycled volatiles and nutrients so that we did not end up like Venus or Mars. Life assisted tectonics through weathering (Rosing *et al.*, 2006). Biology partitioned C and S between the crust and mantle.

Terrestrial organic evolution is a mixed blessing for inferring what happened on other planets. One cannot extrapolate cosmically from the period where we have a good geological record. Life has evolved to be fit for the conditions it actually experienced during the Earth's history. For example, the Earth has the right amount of water so that tectonics and erosion both tend to generate surfaces near sea level (Sleep, 2005). Abundant shallow seas made the transition to land easy. Overall, evolution for fitness to current conditions produces the illusions of design and providence. Any intelligent organism, as a survivor, will find that its personal family tree and its species have had a harrowing history, giving the illusion of good fortune to the point of miracle.

Past performance does not imply future results. Tectonic vigor wanes. Our Sun waxes. Unless a high-tech society intervenes, our greenhouse will runaway because water vapor is a potent greenhouse gas (e.g., Kasting and Catling, 2003). An increase in global sea-surface temperature produces more water vapor and hence a hotter climate. Above a threshold the feedback is unstable. Our life-giving ocean will be our curse.

Tectonics may extricate us from disaster by jettisoning the ocean in the mantle. The mass balance is reasonable. Right now, basalt covers about 90% of the ocean's surface and serpentinite covers the other 10%. Basalt hydrates at ridge axes to form greenstone. This is a modest water sink. An equivalent thickness of 1–2 km is hydrated to 3% water by mass or 10% by volume (Staudigel, 2003; Rüpke *et al.*, 2004). The basalt flux by slabs is equivalent to 100–200 m of ocean depth globally every 170 My. Serpentinite is ~40% water by volume (Rüpke *et al.*, 2004). Its 10% of the seafloor carries an equivalent of 40–80 m every 170 My. In total, it takes 1.5–3.0

billion years to subduct the ocean equivalent thickness (2500 m) of water. However, most of this water returns to the surface in arc volcanoes (Wallace, 2005).

A prolonged period of sluggish seafloor spreading occurs in the models (**Figures 1–3**). The Earth may transition to rather than jump to the stagnant-lid mode of convection. The cool mantle during this epoch implies that much of the seafloor will be serpentinite and that any basaltic crust is highly fractured. The mantle will be too cool for most arcs to be an effective water-return mechanism. The spreading rate at –0.9 Ga in the model is still 83% of the current rate at the transition. A fully serpentinized ocean would subduct the available water in 0.65–1.3 Ga at that rate.

The Earth will resemble the fictional planet *Dune* once the oceans have been subducted. There will still be some groundwater. There will be open water and ice only at the poles. This cold trap will set the global dew point to a low temperature. The meager amount of water vapor will be an ineffective greenhouse gas. Our descendants may well help these processes by pumping water into serpentinite and harvesting H_2 gas from the effluent.

On the other hand, plate tectonics may end suddenly and soon. In that case, erosion will bevel the continents. Some volcanoes and dry land may persist, but not the bounty associated with active tectonics. We will not need a set to remake *Waterworld*.

9.06.8 Conclusions and Musings

Geologists' view of the ancient Earth and their repertoire of methods have changed beyond recognition since 1963. Geochemistry and geochronology were mostly aids to mapping rather than powerful quantitative techniques directed at physical processes. The idea that high-temperature metamorphism was exclusively Pre-Cambrian flourished. There was a general hesitancy for considering geology beyond a local scale. Physics did not seem relevant. Geosynclines produced orogenies when and where they were wont to do so.

Geodynamic models of the early Earth were generic in the 1970s. They did not utilize available information including the presence of high-temperature komatiite lavas in the Archean. 'Don't think' signs remained posted around the Archean 'basement complex' until the late 1970s. For example, a senior faculty member criticized the author for pointing out transposed dikes on a departmental field trip to the Superior Province. These features, when of venerable Archean age, were to be called by the uninformative generic term 'schieren'. Brian Windley visited Northwestern right after this trip. He had much better, more deformed, and far older examples in Greenland that he traced into intact dikes. We began to think about the Archean in a quantitative physical manner.

The high-hanging fruits of years of careful fieldwork with geochronology and geochemistry are now in the basket. Geologists often recognize the basic features of plate processes when they look in the Archean. However, Archean tectonics did differ from the modern process. The continental crust frequently acted as a fluid. Dense mafic rocks foundered into the lower crust. Broad areas like the Minto Block in Canada and the eastern Pilbara craton were dominated by vertical tectonics.

There is enough information to rationally discuss the evolution of tectonic rates. Tiny zircon crystals show that continent-like material formed and survived soon after the moon-forming impact. The statistics of their ages indicate that the events punctuated the local evolution of the crust, just as they do now. The rate of crustal overturn was probably higher than present by as much as a factor of 10. The heat flow may have been as much as a factor of $\sqrt{10} = \sim 3$ higher.

By 3 Ga, the interior was less than 200 K hotter than at present. There is more record and it is easier to talk about rates. The answer may not be satisfying. The global rate of plate tectonics was comparable to the present rate. It remained so thereafter.

Chemically buoyant continental lithospheric mantle kept some overlying continental crust out of harm's way. Its basal region sequestered a record of the conditions at the time of its formation that ascends to the surface as xenoliths. Geochemists are now examining this treasure trove. Their work establishes the antiquity of subduction. It is yet to provide tight constraint on the variation of mantle temperature over time.

The simple quantitative models in this chapter provide heat balance constraints and a guide to possibilities. The geological record is a better master. The transition from mush ocean to plate tectonics is complicated. Before the transition, partly molten material at the base of the mush ocean facilitated convection in the underlying mantle and foundering of cooled mafic crust. After the transition, the need for the base of the

oceanic crust to freeze hindered subduction. The Earth could have lingered over a billion years at this transition. A semantic discussion about what constitutes plate tectonics is unproductive.

Further quantification from geodynamics requires obtaining the globally averaged heat flow by much better than a factor of 2. We need to know whether global heat flow varies continuously and monotonically; that is, does interior temperature and the heat flow–temperature relationship have branches and sharp transitions? These tasks are not simple. Archean tectonics are more complicated than modern plates or even an early vigorous mush ocean. There is meager preservation of the oceanic record. Continental tectonics often involved fluid-like deformation in the crust. Geodynamicists do not have quantitative understanding of analogous vertical tectonic regions like the Basin and Range. The feedback between global heat flow and continental area has only recently been studied numerically (Lenardic *et al.*, 2005).

Current dynamic models do not even do a good job of representing the spontaneous formation of modern plate boundaries. A damage rheology where faults form and heal is a minimum requirement (Tackley, 2000a, 2000b). In this case, the instantaneous rheology implies an increase in stress for an increase in strain rate. The steady-state rheology is strain-rate strengthening below a critical strain rate and 'yield' stress. It is strain rate weakening above that stress and strain rate. This represents the observation that plate boundaries are weaker than typical rocks failing in friction (Zoback and Townend, 2001). The numerical models will need to nicely represent 'normal' plate boundaries, hot-spot ridges like Iceland, mobile continental crust, arc–continent collisions, oceanic subplate boundaries, and oceanic plateaus before they can be exported to the ancient Earth.

We generalize from the observation that plate-like behavior occurred on the Earth for much of its history to infer that plate tectonics is a viable candidate mechanism on other worlds. Pressure-release melting clearly occurs over an extensive depth range in the low gravity of Mars. The base of the mush ocean would stabilize at $\sim 150\,\mathrm{km}/0.4 = 375\,\mathrm{km}$ depth. The 'room' problem for basaltic crust to subduct into the mush is less severe than on the Earth. However, quantitative geodynamics is not ready for extraterrestrial export to the early active history of Mars and Venus. Rather with exploration, geodynamics is likely to import calibration from the excellent geological record of Mars.

The Cretaceous–Tertiary asteroid impact linked geology, astronomy, and biology. The conditions following an ocean-boiling impact are even more foreign to the peaceful environments studied by traditional paleontology. Geology now provides a shopping list of feasible conditions for the early Earth. Molecular biology provides eyewitness accounts in the genomes of extant organisms. It has the potential to resurrect information lost from our rock record.

Acknowledgments

Amy Weislogel pointed out and provided her detrital zircon data. This work was supported by NSF grant EAR-0406658. This work was performed as part of collaboration with the NASA Astrobiology Institute Virtual Planetary Laboratory Lead Team.

Appendix 1: Thermal Models

Figures 1–3 represent generalizable features of the Earth's thermal evolution. The calculations represent realizable cases. We made no effort to tweak the model parameters other than adjusting the monotonic model so that the current potential temperature is 1300°C and the current heat flow is $0.07\,\mathrm{W\,m^{-2}}$. (Petrologists do much better with the relative variations of temperature than they do with the absolute temperature (Putirka, 2005; Herzberg, 2007)). The author uses 1300°C to maintain consistency with his earlier papers.) Heat flow is in $\mathrm{W\,m^{-2}}$ and age B is billion years in the following equations. The radioactive heat production is

$$q_{\mathrm{rad}} = 0.035 \cdot 2^{B/2.5} \qquad [29]$$

The rate of temperature change per billion years is 180 K per billion year at a net heat flow of $0.07\,\mathrm{W\,m^{-2}}$. Mush-ocean heat flow is

$$q = 0.3\exp\left[\frac{T - 1500^{\circ}\mathrm{C}}{150\,\mathrm{K}}\right] \qquad [30]$$

This corresponds to $T_{\eta} = 50\,\mathrm{K}$. Plate tectonic heat flow is the maximum of

$$q = 0.0934 - 0.0234\left[\frac{T - 1400^{\circ}\mathrm{C}}{100\,\mathrm{K}}\right]^2 \qquad [31]$$

and 0.02 W m^{-2}. This provides a weak temperature dependence with a maximum at 1400°C. The extra digits tweaked the model to the assumed current conditions. The stagnant-lid heat flow is

$$q = 0.02\exp\left[\frac{T - 1300^{\circ}\mathrm{C}}{150\,\mathrm{K}}\right] \qquad [32]$$

This also corresponds to $T_\eta = 50$ K. The branch jumps on cooling are 1500°C for mush ocean to plates and 1250°C for plates to stagnant lid. The monotonic model remained at the transition temperature until radioactive heat generation was lower than the heat flow of the cooler mode. The nonmonotonic model heated up in the plate model and jumped to mush ocean at 1600°C. No jump back to plates occurred in this model, as the interior did not heat up much.

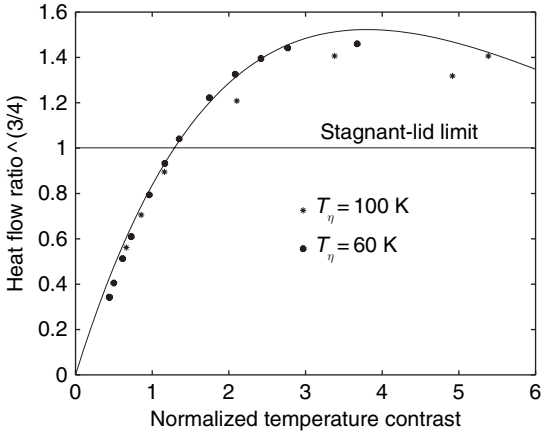

Figure 9 Numerical results for convection beneath a free-slip conducting lid in normalized heat flow and normal rheological temperature contrast *A*. The author varied the rheological temperature contrast to show that the scaling relationship applies.

Appendix 2: Convection beneath Free-Slip Lid

As envisioned, solid-state convection within the underlying mantle was the process that limited heat flow through the mush ocean. Magma entering the mush ocean froze. The temperature at the base of the mush ocean was thus less than that of the entering magma and of the ambient mantle. The difference between this temperature and the temperature of the ambient mantle drove mantle convection. The difference was probably a few hundred kelvin. This appendix shows that the heat flow was insensitive to this rheological temperature contrast ΔT_M. The author defines the dimensionless variable $A \equiv \Delta T_M / T_\eta$ to compact notation.

Here the numerically simple situation of convection beneath a conductive layer with a free-slip bottom as a proxy for a complicated mush chamber is used (**Figure 9**). The numerical method is discusssed at the end of this appendix. From [8], the heat flow should scale to $A^{4/3}$ when the temperature contrast is smaller than 1. The stagnant-lid heat flow in [8] provides a natural scaling. This normalized heat flow may be greater than 1 as the upper part of the rheological boundary layer flows efficiently. The eyeball curve in the form of the linear rheology part of [18] is

$$\left[\frac{q_\mathrm{CL}}{q_\mathrm{SL}}\right]^{3/4} = \left[\frac{A}{3}\right]\exp[(4.5 - A)/3.8] \qquad [33]$$

The heat flow reaches a maximum at a normalized rheological temperature contrast of ~3.5. The transition to ordinary stagnant-lid convection occurs at higher values. Solomatov and Moresi (2000) give the transition at a normalized contrast of 8 for convection beneath a free-slip isothermal boundary. The curve [33] extrapolates to 1 at 8.5, compatible with this constraint.

The heat flow is slightly greater than the stagnant-lid limit over a broad range of rheological temperature contrast. One thus does not have to know the details of the gabbroic mush to compute the stagnant-lid heat flow. One does have to add the contribution of subduction of basaltic slabs into the mantle. Both the mush-ocean parametrization (29) and the stagnant-lid parametrization (31) have the form of [8] with a ratio of 3.95, rather than ~1.5 in [33]; that is, we have implicitly included a significant slab contribution in the parametrized model.

The author uses two-dimensional (2-D) thermal models to find the scaling relationship [33] using the stream-function code by Sleep (2002, 2003, 2005). We impose a conducting lid from 197.5 km depth to the surface where it was 0°C. The models have a 5 km grid. We define temperature at integers times 5 km points in depth and horizontal coordinate. We define the stream function at integer times 5 km plus 2.5 km points. This boundary condition naturally applies at stream function points. We apply free-slip boundary conditions where the vertical velocity was zero and the horizontal shear traction zero to represent a lubricated base of the conducting lid.

The domain of the calculation is 900 km wide. We apply free-slip mechanical boundary conditions at each end and no horizontal heat flow as a thermal boundary condition. We applied a permeable bottom boundary condition at 500 km depth to represent a large underlying adiabatic region. Fluid enters the domain at the potential temperature of 1300°C. There is constant pressure at the boundary so that it does no work on the domain of the model. There is also no horizontal velocity at the boundary.

We did not vary well-constrained parameters in our generic models. These include the thermal expansion coefficient $\alpha = 3 \times 10^{-5}\,\mathrm{K}^{-1}$, volume specific heat $\rho C = 4 \times 10^{6}\,\mathrm{J\,m}^{-3}\,\mathrm{K}^{-1}$, thermal conductivity $k = 3\,\mathrm{W\,m}^{-1}\,\mathrm{K}^{-1}$, the potential temperature of the mantle adiabat $T_L = 1300°\mathrm{C}$, the density $\rho = 3400\,\mathrm{kg\,m}^{-3}$, and the acceleration of gravity $9.8\,\mathrm{m\,s}^{-2}$.

This situation is also relevant to upper boundary layers in a stratified magma chamber and convection within D'' if it is chemically denser and more viscous than the overlying mantle.

References

Abbott DL, Burgess L, Longhi J, and Smith WHF (1994) An empirical thermal history of the Earth's upper mantle. *Journal of Geophysical Research* 99: 13835–13850.

Araki T, Enomoto S, Furuno K, *et al.* (2005) Experimental investigation of geologically produced antineutrinos with KamLAND. *Nature* 436: 499–503.

Arndt N (2003) Komatiites, kimberlites, and boninites. *Journal of Geophysical Research* 108: (doi:10.1029/2002JB002157).

Atwater T (1970) Implications of plate tectonics for Cenozoic tectonic evolution of Western North America. *Geological Society of America Bulletin* 81: 3513–3536.

Bédard JH, Brouillette P, Madore L, and Berclaz A (2003) Archaean cratonization and deformation in the northern Superior Province, Canada: An evaluation of plate tectonic versus vertical tectonic models. *Precambrian Research* 127: 61–87.

Blake TS, Buick R, Brown SJA, and Barley ME (2004) Geochronology of a Late Archaean flood basalt province in the Pilbara Craton, Australia: Constraints on basin evolution, volcanic and sedimentary accumulation, and continental drift rates. *Precambrian Research* 133: 143–173.

Bleeker W (2003) The late Archean record: A puzzle in *c*. 35 pieces. *Lithos* 71: 99–134.

Burke K and Kidd WSF (1978) Were Archean continental geothermal gradients much steeper than those of today? *Nature* 272: 240–241.

Canil D (2004) Mildly incompatible elements in peridotites and the origins of mantle lithosphere. *Lithos* 77: 375–393.

Cavosie AJ, Wilde SA, Liu D, Weiblen PW, and Valley JW (2004) Internal zoning and U–Th–Pb chemistry of Jack Hills detrital zircons: A mineral record of early Archean to Mesoproterozoic (4348–1576 Ma) magmatism. *Precambrian Research* 135: 251–279.

Chen SF, Witt WK, and Liu SF (2001) Transpression and restraining jogs in the northeastern Yilgarn craton, western Australia. *Precambrian Research* 106: 309–328.

Condie KC and Benn K (2006) Archean geodynamics: Similar to or different from modern geodynamics. In: Benn K, Mareschal J-C, and Condie KC (eds.) *Geophysical Monograph Series 164: Archean Geodynamics and Environments*, pp. 47–59. Washington, DC: American Geophysical Union.

Davaille A and Jaupart C (1993a) Thermal convection in lava lakes. *Geophysical Research Letters* 20: 1827–1830.

Davaille A and Jaupart C (1993b) Transient high-Rayleigh-number thermal convection with large viscosity variations. *Journal of Fluid Mechanics* 253: 141–166.

Davaille A and Jaupart C (1994) The onset of thermal convection in fluids with temperature-dependent viscosity: Application to the oceanic mantle. *Journal of Geophysical Research* 99: 19853–19866.

Davies GF (1992) On the emergence of plate tectonics. *Geology* 20: 963–966.

de Ronde CEJ and de Wit MJ (1994) Tectonic history of the Barberton greenstone belt, South Africa: 490 million years of Archean crustal evolution. *Tectonics* 13: 983–1005.

de Ronde CEJ and Kamo SL (2000) An Archean arc–arc collision event: A short-lived (Ca 3 Myr) episode, Weltevreden area, Barbarton greenstone belt, South Africa. *Journal of African Earth Sciences* 30: 219–248.

Dick HJB, Lin J, and Schouten H (2003) An ultraslow-spreading class of ocean ridge. *Nature* 426: 405–412.

Doin M-P, Fleitout L, and Christensen U (1997) Mantle convection and stability of depleted and undepleted continental lithosphere. *Journal of Geophysical Research* 102: 2771–2787.

Dunn SJ, Nemchin AA, Cawood PA, and Pidgeon RT (2005) Provenance record of the Jack Hills metasedimentary belt: Source of the Earth's oldest zircons. *Precambrian Research* 138: 235–254.

England P and Bickle M (1984) Continental thermal and tectonic regimes during the Archean. *Journal of Geology* 92: 353–367.

Farquhar J, Wing BA, McKeegan KD, Harris JW, Cartigny P, and Thiemens MH (2002) Mass-independent sulfur of inclusions in diamond and sulfur recycling on the early Earth. *Science* 298: 2369–2372.

Fiorentini G, Lissia M, Mantovani F, and Vannucci R (2005) Geo-neutrinos: A new probe of Earth's interior. *Earth and Planetary Science Letters* 238: 235–247.

Friend CRL, Bennett VC, and Nutman AP (2002) Abyssal peridotites >3800 Ma from southern West Greenland: Field relationships, petrography, geochronology, whole-rock and mineral chemistry of dunite and harzburgite inclusions in the Itsaq Gneiss Complex. *Contributions to Mineralogy and Petrology* 143: 71–92.

Furnes H, de Wit M, Staudigel H, Rosing M, and Muehlenbachs K (2007) A vestige of Earth's oldest ophidite. *Science* 315: 1704–1707.

Galer SJG and Mezger K (1998) Metamorphism denudation and sea level in the Archean and cooling of the Earth. *Precambrian Research* 92: 387–412.

Grassineau NV, Abell PWU, Fowler CMR, and Nisbet EG (2005) Distinguishing biological from hydrothermal signatures via sulphur and carbon isotopes. In: Archaean mineralizations at 3.8 and 2.7 Ga. In: McDonald I, Boyce AL, Butler IB, Herrington RJ, and Polya DA (eds.) *Geological Society London, Special Publication 248: Mineral Deposits and Earth Evolution*, pp. 195–212. Bath, UK: Geological Society Publishing House.

Grove TL and Parman SW (2004) Thermal evolution of the Earth as recorded by komatiites. *Earth and Planetary Science Letters* 219: 173–187.

Harrison TM, Blichert-Toft J, Muller W, Albarede F, Holden P, and Mojzsis SJ (2005) Heterogeneous hadean hafnium: Evidence of continental crust at 4.4 to 4.5 Ga. *Science* 310: 1947–1950.

Herzberg C, Asimow PD, Arndt N, *et al.* (2007) Temperatures in ambient mantle and plumes: Constraints from basalts, picrites and komatiites. *Geochemistry Geophysics Geosystems* 8: Q02006.

Hickman AH (2004) Two contrasting granite-greenstone terranes in the Pilbara Craton, Australia: Evidence for vertical and horizontal tectonic regimes prior to 2900. *Precambrian Research* 131: 153–172.

Hofmann A and Kusky TM (2004) The Belingwe Greenstone belt: Ensialic or oceanic? In: Kusky TM (ed.) *Developments in Precambrian Geology, 13: Precambrian Ophiolites and Related Rocks*, pp. 487–538. Amsterdam: Elsevier.

Huebeck C and Lowe DR (1994) Late syndepositional deformation and detachment tectonics in the Barberton Greenstone Belt, South Africa. *Tectonics* 13: 1514–1536.

Hurley PM and Rand JR (1969) Pre-drift continental nuclei. *Science* 164: 1229–1242.

Jacob DE, Schmickler B, and Schulze DJ (2003) Trace element geochemistry of coesite-bearing eclogites from the Roberts Victor kimberlite, Kaapvaal craton. *Lithos* 71: 337–351.

Kasting JF and Catling D (2003) Evolution of a habitable planet. *Annual Review of Astronomy and Astrophysics* 41: 429–463.

Kisters AFM, Stevens G, Dziggel A, and Armstrong RA (2003) Extensional detachment faulting and core-complex formation in the southern Barberton granite-greenstone terrain, South Africa: Evidence for a 3.2 Ga orogenic collapse. *Precambrian Research* 127: 355–378.

Kitijima K, Maruyama S, Utsunomiya S, and Liou JG (2001) Seafloor hydrothermal alteration at an Archaean mid-ocean ridge. *Journal of Metamorphic Geology* 19: 581–597.

Klein EM (2003) Geochemistry of the igneous oceanic crust. In: Holland HD and Turekian KK (eds.) *Treatise on Geochemistry: The Crust,* vol. 3 (Rudnick RL), ch. 3.13, pp. 433–463. Amsterdam: Elsevier.

Klein EM and Langmuir CH (1987) Global correlations of ocean ridge basalt chemistry with axial depth and crustal thickness. *Journal of Geophysical Research* 92: 8089–8115.

Korenaga J (2006) Archean geodynamics and the thermal evolution of the Earth. In: Benn K, Mareschal J-C, and Condie KC (eds.) *Geophysical Monograph Series 164: Archean Geodynamics and Environments*, pp. 7–32. Washington, DC: American Geophysical Union.

Kusky TM, Li JH, and Tucker RD (2001) The archean dongwanzi ophiolite complex, North China craton: 2.505-billion-year-old oceanic crust and mantle. *Science* 292: 1142–1145.

Lenardic A, Moresi LN, Jellinek AM, and Manga M (2005) Continental insulation, mantle cooling, and the surface area of oceans and continents. *Earth and Planetary Science Letters* 234: 317–333.

Lenardic A, Moresi L-N, and Mühlhaus H (2003) Longevity and stability of cratonic lithosphere: Insights from numerical simulations of coupled mantle convection and continental tectonics. *Journal of Geophysical Research* 108: (doi:10.1029/2002JB001859).

Liebske C, Schmickler B, Terasaki H, *et al.* (2005) Viscosity of peridotite liquid up to 13 GPa: Implications for magma ocean viscosities. *Earth and Planetary Science Letters* 240: 589–604.

Lin SF (2005) Synchronous vertical and horizontal tectonism in the Neoarchean: Kinematic evidence from a synclinal keel in the northwestern Superior craton, Canada. *Precambrian Research* 139: 181–194.

McKenzie D and Bickle MJ (1988) The volume and composition of melt generated by extension of the lithosphere. *Journal of Petrology* 29: 625–679.

Menzies AH, Carlson RW, Shirey SB, and Gurney JJ (2003) Re–Os systematics of diamond-bearing eclogites from the Newlands kimberlite. *Lithos* 71: 323–336.

Molnar P and Tapponnier P (1975) Cenozoic tectonics of Asia: Effects of a continental collision. *Science* 189: 419–425.

Moores EM (2002) Pre-1 Ga (pre Rodinian) ophiolites: Their tectonic and environmental implications. *Geological Society of America Bulletin* 114: 80–95.

Morgan JK, Moore GF, and Clague DA (2003) Slope failure and volcanic spreading along the submarine south flank of Kilauea volcano, Hawaii. *Journal of Geophysical Research* 108: 2415 (doi:10.1029/2003JB002411).

Nakamura K and Kato Y (2004) Carbonatization of oceanic crust by the seafloor hydrothermal activity and its significance as a CO_2 sink in the Early Archean. *Geochimica et Cosmochimica Acta* 68: 4595–4618.

Nisbet EG (1991) *Living Earth: A Short History of Life and Its Home*, 237 pp. London: Harper Collins Academic.

Okubo PG, Benz HM, and Chouet BA (1997) Imaging the crustal magma sources beneath Mauna Loa and Kilauea volcanoes, Hawaii. *Geology* 25: 867–870.

O'Neill C and Wyman DA (2006) Geodynamic modeling of Late Archean subduction: Pressure-temperature constraints from greenstone belt diamond deposits. In: Benn K, Mareschal J-C, and Condie KC (eds.) *Geophysical Monograph Series 164: Archean Geodynamics and Environments*, pp. 177–188. Washington, DC: American Geophysical Union.

Pavlov A and Kasting JF (2002) Mass-independent fractionation of sulfur isotopes in Archean sediments: Strong evidence for an anoxic Archean atmosphere. *Astrobiology* 2: 27–41.

Plank T and Langmuir CH (1992) Effects of the melting regime on the composition of the oceanic crust. *Journal of Geophysical Research* 97: 19749–19770.

Polat A and Kerrich R (2006) Reading the geochemical fingerprints of Archean hot subduction volcanic rocks: Evidence for accretion and crustal recycling in a mobile tectonic regime. In: Benn K, Mareschal J-C, and Condie KC (eds.) *Geophysical Monograph Series 164: Archean Geodynamics and Environments*, pp. 189–213. Washington, DC: American Geophysical Union.

Putirka KD (2005) Mantle potential temperatures at Hawaii, Iceland, and the mid-ocean ridge system, as inferred from olivine phenocrysts: Evidence for thermally driven mantle plumes. *Geochemistry Geophysics Geosystems* 6: Q05L08.

Ritzwoller MH, Shapiro NM, and Leahy GM (2003) A resolved mantle anomaly as the cause of the Australian–Antarctic Discordance. *Journal of Geophysical Research* 108: B12, 2559.

Rosing MT, Bird DK, Sleep NH, Glassley W, and Albarede F (2006) The rise of continents – An essay on the geologic consequences of photosynthesis. *Palaeogeography Palaeoclimatology Palaeoecology* 232(2-4): 99–113.

Rüpke LH, Phipps Morgan J, Hort M, and Connolly JAD (2004) Serpentine and the subduction zone water cycle. *Earth and Planetary Science Letters* 223: 17–34.

Ryder G (2002) Mass flux in the ancient Earth–Moon system and benign implications for the origin of life on Earth. *Journal of Geophysical Research* 107(E4): 5022.

Saltzer RL, Chatterjee N, and Grove TL (2001) The spatial distribution of garnets and pyroxenes in mantle peridoties: Pressure-temperaturer history of peridotites from the Kaapvaal craton. *Journal of Petrology* 42: 2215–2229.

Schulze DJ, Harte B, Valley JW, Brenan JM, and Channer DM de R (2003a) Extreme crustal oxygen isotope signatures preserved in coesite in diamond. *Nature* 423: 68–70.

Schulze DJ, Valley JW, Spicuzza MJ, and Channer DM de R (2003b) The oxygen isotope composition of eclogitic and

peridotitic garnet xenoliths from the La Ceniza kimberlite, Guaniamo, Venezuela. *International Geology Review* 45: 968–975.

Sinton JM and Detrick RS (1992) Midocean ridge magma chambers. *Journal of Geophysical Research* 97: 197–216.

Sleep NH (1979) Thermal history and degassing of the Earth: Some simple calculations. *Journal of Geology* 87: 671–686.

Sleep NH (1992) Archean plate-tectonics – what can be learned from continental geology. *Canadian Journal of Earth Sciences* 29: 2066–2071.

Sleep NH (2000) Evolution of the mode of convection within terrestrial planets. *Journal of Geophysical Research* 105: 17563–17578.

Sleep NH (2002) Local lithospheric relief associated with fracture zones and ponded plume material. *Geochemistry Geophysics Geosystems* 3: 8506 (doi:2001GC000376).

Sleep NH (2003) Survival of Archean cratonal lithosphere. *Journal of Geophysical Research* 108 (doi:10.1029/2001JB000169).

Sleep NH (2005) Evolution of continental lithosphere. *Annual Review of Earth and Planetary Science* 33: 369–393.

Sleep NH (2006) Strategy for applying neutrino geophysics to the earth sciences including planetary habitability. *Earth Moon and Planet* 99: 343–358.

Sleep NH and Windley BF (1982) Archean plate tectonics: Constraints and inferences. *Journal of Geology* 90: 363–379.

Sleep NH and Zahnle K (1998) Refugia from asteroid impacts on early Mars and the early Earth. *Journal of Geophysical Research* 103: 28529–28544.

Sleep NH and Zahnle K (2001) Carbon dioxide cycling and implications for climate on ancient Earth. *Journal of Geophysical Research* 106: 1373–1399.

Sleep NH, Zahnle K, and Neuhoff PS (2001) Initiation of clement surface conditions on the early Earth. *PNAS* 98: 3666–3672.

Sobolev AV, Hofmann AW, Sobolev SV, and Nikogosian IK (2005) An olivine-free mantle source of Hawaiian shield basalts. *Nature* 434: 590–597.

Solomatov VS (1995) Scaling of temperature- and stress-dependent viscosity convection. *Physics of Fluids* 7: 266–274.

Solomatov VS (2004) Initiation of subduction by small-scale convection. *Journal of Geophysical Research* 109: B01412.

Solomatov VS and Moresi L-N (2000) Scaling of time-dependent stagnant lid convection: Application to small-scale convection on Earth and other terrestrial planets. *Journal of Geophysical Research* 105: 21795–21817.

Staudigel H (2003) Hydrothermal alteration processes in the oceanic crust. In: Holland HD and Turekian KK (eds.) *Treatise on Geochemistry: The Crust*, vol. 3 (Rudnick RL), pp. 511–535. Amsterdam: Elsevier.

Stern RJ (2005) Evidence from ophiolites, blueschists, and ultrahigh-pressure metamorphic terranes that the modern episode of subduction tectonics began in Neoproterozoic time. *Geology* 33: 557–560.

Stevenson DJ (2003) Styles of mantle convection and their influence on planetary evolution. *Comptes Rendus Geoscience* 335: 99–111.

Tackley PJ (2000a) Self-consistent generation of tectonic plates in time-dependent, three-dimensional mantle convection simulations. Part 1: Pseudoplastic yielding. *Geochemistry Geophysics Geosystems* 1 (doi:10.1029/2000GC000036).

Tackley PJ (2000b) Self-consistent generation of tectonic plates in time-dependent, three-dimensional mantle convection simulations. Part 2: Strain weakening and asthenosphere. *Geochemistry Geophysics Geosystems* 1 (doi:10.1029/2000GC000043).

Thom R (1983) *Parabolas et Catastrophes* 193 pp. Paris Flammarion.

Tozer DC (1970) Factors determining the temperature evolution of thermally convecting Earth models. *Physics of the Earth and Planetary Interiors* 2: 393–398.

Turcotte DL and Schubert G (1982) *Geodynamics: Applications of Continuum Physics to Geological Problems*, 450 pp. New York: John Wiley.

Van Kranendonk MJ, Collins WJ, Hickman A, and Pawley MJ (2004) Critical tests of vertical vs. horizontal tectonic models for the Archaean East Pilbara Granite-Greenstone Terrane, Pilbara Craton, western Australia. *Precambrian Research* 131: 173–211.

van Thienen P, Vlaar NJ, and van den Berg AP (2004) Plate tectonics on the terrestrial planets. *Physics of the Earth and Planetary Interiors* 142: 61–74.

Wallace PJ (2005) Volatiles in subduction zone magmas: Concentrations and fluxes based on melt inclusion and volcanic gas data. *Journal of Volcanology and Geothermal Research* 140: 217–240.

Weislogel AL, Graham SA, Chang EZ, Wooden JL, Gehrels GE, and Yang H (2006) Detrital - zircon provenance of the Late Triassic Songpan - Ganzi complex: Sedimentary record of collision of the North and South China blocks. *Geology* 34(2): 97–100.

White RS, McKenzie D, and O'Nions RK (1992) Oceanic crustal thickness from seismic measurements and rare Earth element inversions. *Journal of Geophysical Research* 97: 19683–19715.

Wilson DS, McCrory PA, and Stanley RG (2005) Implications of volcanism in coastal California for the Neogene deformation history of Western North America. *Tectonics* 24(3): TC3008.

Zahnle K, Arndt N, Cockell C, *et al.* (2007) Emergence of a habitable planet. *Space Science Review* (in press).

Zahnle K and Sleep NH (2006) Impacts and the early evolution of life. In: Thomas PJ, Hicks RD, Chyba CF, and McKay CP (eds.) *Comets and the Origin and Evolution of Life,* 2nd edn., pp. 207–251. Berlin: Springer.

Zatman S, Gordon RG, and Mutnuri K (2005) Dynamics of diffuse oceanic plate boundaries: Insensitivity to rheology. *Geophysical Journal International* 162: 239–248.

Zoback MD and Townend J (2001) Implications of hydrostatic pore pressures and high crustal strength for the deformation of intraplate lithosphere. *Tectonophysics* 336: 19–30.